

V1-Origin Bidirectional Plasticity in Visual Thalamo-Ventral Pathway and Its Contribution to Saliency Detection of Dynamic Visual Inputs

Shang Feng, Zhichang Cui, Zhengqi Han, Hongjian Li, and Hongbo Yu

School of Life Sciences, State Key Laboratory of Medical Neurobiology, Collaborative Innovation Centre for Brain Science, Fudan University, Shanghai 200433, China

Visual neural plasticity and V1 saliency detection are vital for efficient coding of dynamically changing visual inputs. However, how does neural plasticity contribute to saliency detection of temporal statistically distributed visual stream remains unclear. Therefore, we adopted randomly presented but unevenly distributed stimuli with multiple orientations and examined the single-unit responses evoked by this biased orientation-adaptation protocol by single-unit recordings in the visual thalamo-ventral pathway of cats (of either sex). We found neuronal responses potentiated when the probability of biased orientation was slightly higher than other nonbiased ones and suppressed when the probability became much higher. This single neuronal short-term bidirectional plasticity is selectively induced by optimal stimuli but is interocularly transferable. It is inducible in LGN, Area 17, and Area 21a with distinct and hierarchically progressive patterns. With the results of latency analysis, receptive field structural test, cortical lesion, and simulations, we suggest this bidirectional plasticity may principally originate from the adaptation competition between excitatory and inhibitory components of V1 neuronal receptive field. In our simulation, above bidirectional plasticity could achieve saliency detection of dynamic visual inputs. These findings demonstrate a rapid probability dependent plasticity on the neural coding of visual stream and suggest its functional role in the efficient coding and saliency detection of dynamic environment.

Key words: Area 21a; LGN; plasticity; primary visual cortex; saliency detection; visual adaptation

Significance Statement

Novel elements within a dynamic visual stream can pop up from the context, which is vital for rapid response to a dynamically changing world. Saliency detection is a promising bottom-up mechanism contributing to efficient selection of visual inputs, wherein visual adaptation also plays a significant role. However, the saliency detection of dynamic visual stream is poorly understood. Here, we found a novel form of visual short-term bidirectional plasticity in multistages of the visual system that contributes to saliency detection of dynamic visual inputs. This bidirectional plasticity may principally originate from the local balance of excitation inhibition in primary visual cortex and propagates to lower and higher visual areas with progressive pattern change. Our findings suggest the excitation-inhibition balance within the visual system contributes to visual efficient coding.

Introduction

Visual adaptation is a continuous alteration of sensitivity to (or perception of) visual inputs (Kohn, 2007; Webster, 2015), reflects the neural modulation of temporal distributed visual inputs, and

has been studied as a probe of visual neural plasticity. Visual adaptation universally exists (in various forms) in visual systems of multiple species with various duration, and minute-level orientation adaptation aftereffects in LGN (Shou et al., 1996), V1 (Patterson et al., 2013), V2 (Lussiez et al., 2021), V4 (Tolias et al., 2005), and MT (Kohn and Movshon, 2004; Patterson et al., 2014b) have been examined to investigate the feature-specific neural plasticity. The propagation of adaptation along ventral or dorsal visual pathway (Cattan et al., 2014; Patterson et al., 2014a; Li et al., 2017) suggests hierarchical interactions through feedforward or feedback mechanisms. By increasing the temporal sparseness of neuronal activities, visual adaptation could contribute to the efficient coding of visual inputs (Clifford et al., 2007; Kohn, 2007; Schwartz et al., 2007; Rieke and Rudd, 2009;

Received Mar. 17, 2022; revised June 12, 2022; accepted July 8, 2022.

Author contributions: S.F. and H.Y. designed research; S.F., Z.C., Z.H., and H.L. performed research; S.F. contributed unpublished reagents/analytic tools; S.F. analyzed data; S.F. wrote the paper.

This work was supported by National Natural Science Foundation of China Grant 31970928, Shanghai Municipal Science and Technology Major Project Grant 2018SHZDXZ01, and Shanghai Key Discipline Foundation Grant B111.

The authors declare no competing financial interests.

Correspondence should be addressed to Hongbo Yu at hongboyu@fudan.edu.cn.

<https://doi.org/10.1523/JNEUROSCI.0539-22.2022>

Copyright © 2022 the authors

Solomon and Kohn, 2014) including popping out a novel stimulus within the visual field (McDermott et al., 2010; Wissig et al., 2013; Dutta et al., 2016), like saliency detection does.

Saliency detection is another way to achieve efficient coding by rapid selection of salient visual targets through bottom-up process and intermediates the encoding and decoding of visual inputs (Li, 2002, 2019). The basic strategy of V1 saliency detection is emphasizing novel (rarely occurred) stimulus and suppressing redundant (frequently occurred) stimulus, and the spatial saliency detection has been extensively studied (Li, 2019). However, the characteristics and neural mechanisms of temporal saliency detection (vital for survival in a dynamically changing world) remained less investigated. Considering that visual adaptation reflects the temporal-coding feature of visual system, examinations on temporal saliency detection might benefit from the visual adaptation mechanism.

The basic visual attributes (like orientation) of dynamic visual inputs could be characterized in a statistical way (Ruderman and Bialek, 1994; Kayser et al., 2003; Torralba and Oliva, 2003; Hyvärinen et al., 2004). Theoretically, by increasing neural response to novel stimulus (low occurrence probability) and decreasing neural response to redundant stimulus (high occurrence probability), temporal saliency detection could be performed in a push-pull manner, just like spatial saliency detection does. However, in classical visual adaptation protocol (for example, top-up adaptation), the occurrence probability of the adaptor is too high to represent the novel stimulus (Kohn and Movshon, 2004; Patterson et al., 2013, 2014a), requiring a more suitable adaptation protocol.

The biased-adaptation protocol is proper for temporal coding investigation on visual inputs of various novelties because its strength is quantified by the occurrence probability difference between adaptor and nonadaptors (thus reflecting the novelty of adaptor) and could be finely chosen. Visual studies using biased-adaptation protocol (Benucci et al., 2013; Dhruv and Carandini, 2014; Snow et al., 2016; Westrick et al., 2016) has increased our knowledge of neural population homeostasis and normalization. However, current pioneering studies mainly adopt a certain fixed occurrence probability and did not investigate its potential contribution to saliency detection.

Therefore, in this study we adopted the biased orientation adaptation with different occurrence probabilities, performed electrophysiological single-unit recording in cats, and unexpectedly found short-term bidirectional plasticity (potentiation at low occurrence probability, and suppression at high occurrence probability) in LGN, Area 17, and Area 21a with a hierarchically progressive pattern change. This novel bidirectional plasticity may originate from the adaptation competition between excitatory and inhibitory components of the V1 neuronal receptive field and could contribute to the saliency detection of temporal statistically distributed visual inputs.

Materials and Methods

Study approval

Data from 13 normal cats of either sex weighing 2.5 ~ 3.5 kg were used in this study. All experiments involving animals were conducted in accordance with guidelines from the National Institutes of Health and were approved by the Animal Care and Use Committee at Fudan University.

Animal preparation

As described in our previous reports (Li et al., 2018), anesthesia was induced with ketamine hydrochloride (20 mg/kg) and sustained by 2.0 ~ 3.0% isoflurane (RWD Life Science) during the surgery. All pressure

points and incised tissues were infiltrated with lidocaine. After the surgery, anesthesia was maintained with 1.0% isoflurane. Cats were paralyzed (gallamine triethiodide, 8 ~ 10 mg/kg/h, i.v.) and artificially respired by a pulmonary pump (catalog #6025, UGO Basile) to maintain end-tidal CO₂ at 3.5 ~ 4.0%. The body temperature of animals was monitored and maintained at 38.0°C throughout the procedure by an automatic temperature control system (catalog #BME-461A, Institute of Biomedical Engineering, Chinese Academy of Medical Sciences). Electroencephalogram and electrocardiogram were monitored continuously to ensure adequate anesthesia. The pupils were dilated with atropine (1%), and the nictitating membranes were retracted with neosynephrine (5%). The eyes were refracted and corrected with contact lenses.

A craniotomy and durotomy were performed at Horsley–Clarke coordinates posterior (P)2 ~ P10 and lateral (L)0 ~ L5 for Area 17 (Li et al., 2017; Meng et al., 2018; Wang et al., 2019), P0 ~ P7 and L9 ~ L16 for Area 21a (Dreher et al., 1993; Wang et al., 2000; Huang et al., 2006; Tong et al., 2011), and anterior (A)5 ~ A7, L8 ~ L10 for dLGN (Li et al., 2018) to allow electrophysiological recordings. Area 21a is located in the middle part of caudal suprasylvian gyrus defined by anatomic connections and retinotopic organization in cats (Van Der Gucht et al., 2001) and bounded medially and caudally by Area 19 and laterally bordered by posteromedial lateral suprasylvian area. dLGN is beneath the cortex surface for 11 ~ 14 mm. A plastic chamber was secured to the skull using dental cement. Extracellular electric signals were recorded by glass-coated tungsten microelectrodes (3 ~ 5 MΩ, FHC).

Cortex ablation was performed during the Area 17 lesion experiment. The whole Area 17 (Horsley–Clarke coordinates P2 ~ P10, L0 ~ L5) was irreversibly inactivated with liquid nitrogen. A Q-tip was immersed in liquid nitrogen and then touched to the exposed cortex several times briefly (Shou et al., 1996; Li et al., 2018). Cortical lesion was verified by Local Field Potential (LFP) recordings before and after liquid nitrogen operation, and no visual evoked LFP was detected after liquid nitrogen operation.

Biased-adaptation protocol

In this work, the biased-adaptation protocol used drifting sinusoidal gratings of different moving directions. Before adaptation, 12 or 24 directions of gratings were presented for 0.5 s with equal probability (10 repetitions for each grating) followed by 0.5 s blank interval. This session is termed Control.

During the standard biased-adaptation session, 12 or 24 directions were also presented for 0.5 s and followed by 0.5 s blank interval while the change was the occurrence probability of each direction. The adaptor was 1, 2, 3, 4, 8, 20, 40, 60, 80, 120 times [biased-adaptation multiple (BAM); 2, 4, 8, 20, 40 for Area 17; 1, 2, 3, 4, 8, 20, 40 for Area 21a; 8, 20, 40, 60, 80, 120 for LGN] more likely to be presented than any nonadaptors. During analysis, biased-adaptation multiples were converted to biased-adaptation probabilities (BAP) for better comparison effect and better compatibility with the other literature. For tests of 12 directions, BAM 0, 1, 2, 3, 4, 8, 20, 40, 60, 80, 120 correspond to BAP 0.08, 0.15, 0.21, 0.27, 0.31, 0.45, 0.66, 0.79, 0.85, 0.88, 0.92; for tests of 24 directions, above BAM corresponds to BAP 0.04, 0.08, 0.12, 0.15, 0.18, 0.28, 0.48, 0.64, 0.73, 0.78, 0.84. The relationship between BAM and BAP could be described as BAP = (1 + BAM)/(N + BAM), where N is the number of directions (12 or 24). It is notable that for Control stimulus, BAP using 12 or 24 directions was 0.08 or 0.04, respectively.

Recovery sessions (consisting of varied numbers of Control stimuli) were inserted following each biased-adaptation session to ensure that tested neurons could recover to their onset (preadaptation) conditions. Therefore, results of every biased-adaptation session could be compared with each other.

Visual stimuli

The visual stimuli were computer generated using MATLAB (MathWorks), Psychtoolbox (Brainard, 1997; Pelli, 1997), and a Visual Graphic Systems graphic board (VGS 5, Cambridge Research Systems). Visual stimuli were presented on a CRT monitor (FlexScan F931, Eizo Nanao), refreshing at 100 Hz, and positioned 57 cm from eyes of the cat. The cats were stimulated binocularly or monocularly (according to different experimental

requirements) with drifting sinusoidal gratings (size, 7° in diameter; directions, 15 or 30° interval across 0 ~ 360°; spatial frequency, 0.1 ~ 2.0 cycle/deg; temporal frequency, 2.0 Hz; contrast, 50 ~ 100%) or full-screen flash (temporal frequency, 1.67 Hz; contrast, 100%) or flashing bars (temporal frequency, 1.67 Hz; contrast, 100%). Full-screen flash and flashing bars were used for neuron search and receptive field locating. For receptive field structural experiments, the display area (stimulation field) of gratings was set to small (1.5–2.5° in diameter) or annular (4° internal and 10° external in diameter) conditions for certain examining purpose. The parameters were adjusted according to the averaged firing rate of each neuron to optimize its response to the stimulus, except for feature selective experiments (during which nonpreferred stimulation parameters were used).

Electrophysiological recording

Single-unit signals were amplified (model 1700, A-M Systems) bandpass filtered (300 ~ 1 kHz for single-unit signals) and digitized at 16.67 kHz using a data acquisition system (CED Micro1401, Cambridge Electronic Design) under the control of Spike2 software (version 6, Cambridge Electronic Design). Recordings consisted of both single-unit and multiunit activity and were sorted off-line. Spikes were sorted by Spike2 software (Cambridge Electronic Design) and analyzed in MATLAB (MathWorks).

Model

Receptive field center-surround adaptation competition model. The receptive field (RF) center-surround adaptation competition model is modified from the classical Difference of Gaussian (DoG) model (Marr and Hildreth, 1980; Birch et al., 2010). The model consists of two Gaussian components (of different signs), representing the center and surround subarea of the RF. The center component (representing the classical receptive field) is stronger and spatially concentrated, whereas the surround component (representing the surround modulation area) is weaker and spatially broader. The summation of center and surround components forms a Mexican-hat shape, which is identical to the classical visual receptive field structure (Angelucci et al., 2017). The neural response y as a function of RF location x is defined as follows:

$$y(x) = a_1 \frac{1}{\sigma_1 \sqrt{2\pi}} e^{\frac{-x^2}{2\sigma_1^2}} + a_2 \frac{1}{\sigma_2 \sqrt{2\pi}} e^{\frac{-x^2}{2\sigma_2^2}},$$

where a is the gain control factor ($a_1 > 0, a_2 < 0$), and σ is the spatial control factor ($\sigma_2 > \sigma_1 > 0$). Subscript 1 represents the RF center component, whereas subscript 2 represents the RF-surround component.

The gain control factor a is exponentially decaying as the adaptation strength increases. The gain control factor a_μ at biased-adaptation probability μ is defined as follows:

$$a_\mu = c \cdot e^{-b\mu} \cdot a_0,$$

where a_0 is the Gaussian gain control factor before adaptation, b is the adaptation decay factor ($b > 0$), c is the adaptation magnitude factor, and μ represents the biased-adaptation probability.

In summary, taking adaptation into consideration, the overall neural response y as a function of RF location x and adaptation strength μ , is defined as follows:

$$y(x, \mu) = c_1 \cdot e^{-b_1\mu} \cdot a_1 \frac{1}{\sigma_1 \sqrt{2\pi}} e^{\frac{-x^2}{2\sigma_1^2}} + c_2 \cdot e^{-b_2\mu} \cdot a_2 \frac{1}{\sigma_2 \sqrt{2\pi}} e^{\frac{-x^2}{2\sigma_2^2}},$$

where a is the Gaussian gain control factor ($a_1 > 0, a_2 < 0$), b is the adaptation decay factor ($b_2 > b_1 > 0$), c is the adaptation magnitude factor ($c_1 > c_2 > 0$), μ represents the biased-adaptation probability, and σ is Gaussian spatial control factor ($\sigma_2 > \sigma_1 > 0$). Subscript 1 represents the RF center component, whereas subscript 2 represents the RF surround component. In this study, curve fits were obtained using the nonlinear least squares method in the Matlab curve-fitting toolbox.

Visual saliency detection model. The visual input field used in the visual saliency detection model is a 16 × 16 matrix, and each cell represents a visual field location. During the visual input stimulation (composed of hundreds of frames), gratings of various orientations appear in these cells (frame by frame, duration is 0.5 s with a 0.5 s blank interval, which is identical to the experimental protocol), and their accumulating occurrence probabilities are calculated. For each cell, every orientation has its own occurrence probability at the current frame, and this occurrence probability is related to the response intensity of a neuron cluster (according to the bidirectional plasticity function mentioned below), whose RFs lie within this cell. Therefore, at every frame, the neural response map of visual field is calculated. At the same time, the saliency map is also acquired by calculating saliency values of each cell. The output of this model is a saliency map, changing with visual inputs over time.

The visual input is divided into three successive phases, initial noise, detection, and ending noise. During the initial and ending noise phases, gratings are randomly displayed without bias. During the detection phase, a stable elliptical contour (formed of gratings) appeared in the visual field while gratings in other cells are randomly displayed.

The bidirectional plasticity function of Area 17 was obtained by the RF center-surround adaptation-competition model described above (fitting result of the population peak response change ratio curve). The bidirectional plasticity function of LGN was obtained by the MATLAB curve-fitting toolbox, using the smoothing spline method (Reinsch, 1967). The smoothing spline method could generate a fitting curve s by minimizing the target value T as follows:

$$T = p \sum_i (y_i - s(x_i))^2 + (1-p) \int \left(\frac{d^2 s}{dx^2} \right)^2 dx,$$

where (ξ, y_i) is the coordinate of the i th point, and p is defined between 0 and 1. In this study, p was set to default setting ($p = 0.0020573904$, automatically chosen by the MATLAB curve-fitting toolbox) for its best fitting quality.

Saliency value was calculated as described in the previous literature (Li, 2019). For cell m , the saliency value S_m is defined as follows:

$$S_m = \frac{\text{Response}_m}{\max(\text{Response}_{\text{other than } m})},$$

where Response_m means the neural response at cell m , and $\text{Response}_{\text{other than } m}$ means neural responses of other cells.

Data Analysis

Poststimulus time histogram. Poststimulus time histograms (PSTHs) are useful for characterizing the dynamics of neuronal response to specific stimulus. In this study, we calculated the PSTH for each neuron by averaging neuronal responses within 500 ms after stimulus onset (bin width = 50 ms). For overall PSTH, responses to all stimuli were used, whereas for stimulus-type-related PSTH (e.g., PSTH of orientation tuning), responses to different stimuli (e.g., different orientation) were averaged separately.

Orientation selectivity. We applied a vector summation method to measure the preferred orientation and orientation selectivity index (OSI) of cortical neurons based on the spike trains associated with each direction and orientation (Li et al., 2017, 2018; Wang et al., 2019) as follows:

$$S = \frac{\sum_k r_k e^{i2\theta_k}}{\sum_k r_k},$$

where θ_k is the direction of k^{th} drifting grating, and r_k is the average firing rate at that orientation. The firing rate of a neuron was averaged from 50 ms to 500 ms after stimulus onset, and spontaneous responses were subtracted from the raw data. The preferred orientation and OSI

are the phase and the amplitude of S , respectively. OSI varies from zero to one, where zero indicates an equal response to all directions, and one indicates a response to only one direction.

For LGN neurons, we also measured the preferred orientation and orientation bias (OB) using a similar method as described above. As LGN neurons are weakly tuned to orientation, responses used for the OSI calculation were recorded at the cutoff spatial frequency ($1/\sqrt{2}$ maximum gain of spatial frequency tuning) as previously reported (Li et al., 2018). According to the previous literature (Hu et al., 2000; Leventhal et al., 2000; Hua et al., 2006), some LGN neurons only exhibited stable orientation bias using the fast Fourier transform (FFT) first harmonic (H1) component of the PSTH evoked by drifting gratings. Therefore, for LGN neurons, we calculated the OB using both mean responses and FFT H1 components. LGN neurons with an OB of ≥ 0.1 were considered significantly orientation sensitive according to circular statistics as the previous literature reported (Levick and Thibos, 1982; Shou and Leventhal, 1989; Li et al., 2018).

The adaptor was then determined at the preferred orientation of the neuron. For neurons without orientation sensitivity (OSI or OB < 0.1), adaptors were randomly chosen.

Ocular dominance index. The Ocular Dominance Index (ODI) of Area 17 neurons was calculated during the interocular transfer experiment based on the previous literature (Cang et al., 2005; Yu et al., 2011; Tong et al., 2016; Wang et al., 2019) as follows:

$$ODI = \frac{R_{Contra} - R_{Ipsi}}{R_{Contra} + R_{Ipsi}},$$

where R_{Contra} means neuronal response to the contralateral eye, and R_{Ipsi} means neuronal response to the ipsilateral eye. ODI ranges from -1 to 1 , where the positive value indicates contralateral bias, and the negative value indicates ipsilateral bias.

Peak response change ratio. To evaluate the magnitude of response change induced by biased adaptation, we calculated the peak response change ratio (%) which is defined as follows:

$$\begin{aligned} &\text{Peak Response Change Ratio} \\ &= \frac{\text{Peak Response}_{post} - \text{Peak Response}_{pre}}{\text{Peak Response}_{pre}} \times 100, \end{aligned}$$

where $\text{Peak Response}_{pre}$ and $\text{Peak Response}_{post}$ are averaged firing rates at the preferred orientation before and after biased adaptation, respectively.

For LGN neurons, we calculated the trained response change ratio (%) to quantify the influence induced by biased adaptation, which is defined as follows:

$$\begin{aligned} &\text{Trained Response Change Ratio} \\ &= \frac{\text{Trained Response}_{post} - \text{Trained Response}_{pre}}{\text{Trained Response}_{pre}} \times 100, \end{aligned}$$

where $\text{Trained Response}_{pre}$ and $\text{Trained Response}_{post}$ are averaged firing rates or the FFT H1 component at the adaptor (see above, Orientation selectivity) before and after biased adaptation, respectively.

Cell classification. Neurons in Area 17 were classified into simple or complex neurons using the well established relative modulation (RM) method based on neural responses of drifting sinusoidal gratings (De Valois et al., 1982; Skottun et al., 1991) as follows:

$$RM = \frac{AC\ Component}{DC\ Component},$$

where **AC component** is the amplitude of the FFT first harmonic component of PSTH, and **DC component** is the averaged firing rate. Neurons whose RM ≥ 1.0 were termed simple, and those with an RM < 1.0 were termed complex.

Neurons in Area 17 were also classified into regular-spiking (RS) or fast-spiking (FS) neurons according to the previous literature. The two criteria based on spike waveforms that were comprehensively used to improve the classification accuracy were (1) the ratio of the second and first peak (P) amplitude (P2/P1; Kuhlman et al., 2011) and (2) the slope (dV/dt) between the second and first peak within an interval of 0.2 ms (Bachatene et al., 2012). Fast-spiking neurons were classified if their P2/P1 ≥ 0.5 and dV/dt $\geq (0.2, 0.6)$, whereas regular-spiking neurons were classified with the P2/P1 < 0.5 and dV/dt $\leq (0.1, 0.2)$.

Latency analysis. Latency analysis was performed for neurons in Area 17s and 21a and LGN by calculating averaged neuronal responses within certain time windows after stimulus onset. Time windows were set to 50 \sim 100, 100 \sim 200, and 200 \sim 500 ms for cortical areas (Area 17 and Area 21a), and 30 \sim 80, 80 \sim 200, and 200 \sim 500 ms for LGN.

Statistics

In this study, unless otherwise indicated, all statistical significance was determined by paired or unpaired Student's *t* test and multiple comparisons corrections (using the false discovery rate method) were performed throughout (Benjamini and Hochberg, 1995); $p < 0.05$ was considered significant (* $p < 0.05$, ** $p < 0.01$, *** $p < 0.001$). All statistical results are Mean \pm SEM, unless otherwise indicated.

In this study, some biased-adaptation probabilities were not tested in certain experiments under the following conditions: (1) To improve the overall recording efficiency of low-intensity adaptation conditions (< 0.3), some high-intensity adaptation conditions (> 0.48) were skipped; (2) a few neurons could not recover to their preadaptation response level after biased-adaptation stimulation, so their subsequent tests were skipped; (3) for Area 21a, during some early exploratory tests, a finer biased-adaptation probability gradient were not used; and (4) for LGN, during some early exploratory tests, extremely high biased-adaptation probabilities (> 0.78) were not used.

During the latency-analysis of this study, outlier data were identified according to strict fixed standards and were excluded from statistical analysis. Data of a neuron within a certain epoch would be identified as outliers if any of the following conditions were met: (1) During the Control stimulation, this neuron was nonresponsive (averaged firing rate = 0 Hz) to stimuli, or (2) during the biased-adaptation stimulation, this neuron was nonresponsive (averaged firing rate = 0 Hz) to stimuli.

Results

Short-term bidirectional plasticity induced by biased-adaptation protocol in Area 17

We performed electrophysiological single-unit recordings in primary visual cortex (Area 17) of cats to investigate the adaptation effect induced by biased-adaptation protocol (Fig. 1A). First, neurons in Area 17 were stimulated by the Control protocol, that is, sinusoidal drifting gratings of 12 or 24 evenly distributed directions, presented for 0.5 s with 0.5 s blank intervals (Fig. 1B, C). Under the Control protocol, neurons in Area 17 exhibited strong orientation selectivity (OSI = 0.47 ± 0.02 , $n = 105$ from 7 cats; OSI, consistent with previous reports; Li et al., 2017).

After that, the biased-adaptation protocol was applied. To induce the adaptation effect, the occurrence probability of the adaptor was significantly higher than the one of the nonadaptor (Fig. 1B), which is similar to previous reports (Benucci et al., 2013; Li et al., 2017). In this article, we chose BAP (the occurrence probability of the adaptor) to quantify the extent of bias in biased adaptation (for Control stimulus using 12 or 24 directions, BAP are 0.08 or 0.04, respectively). To quantify the extent of influence induced by biased adaptation, we calculated the peak response change ratio of individual neurons based on preadaptation peak response (see above, Materials and Methods). To thoroughly study how biased adaptation influences neurons in Area 17, we set the BAP gradient (0.12 \sim 0.79) to investigate the effects on peak response change ratio.

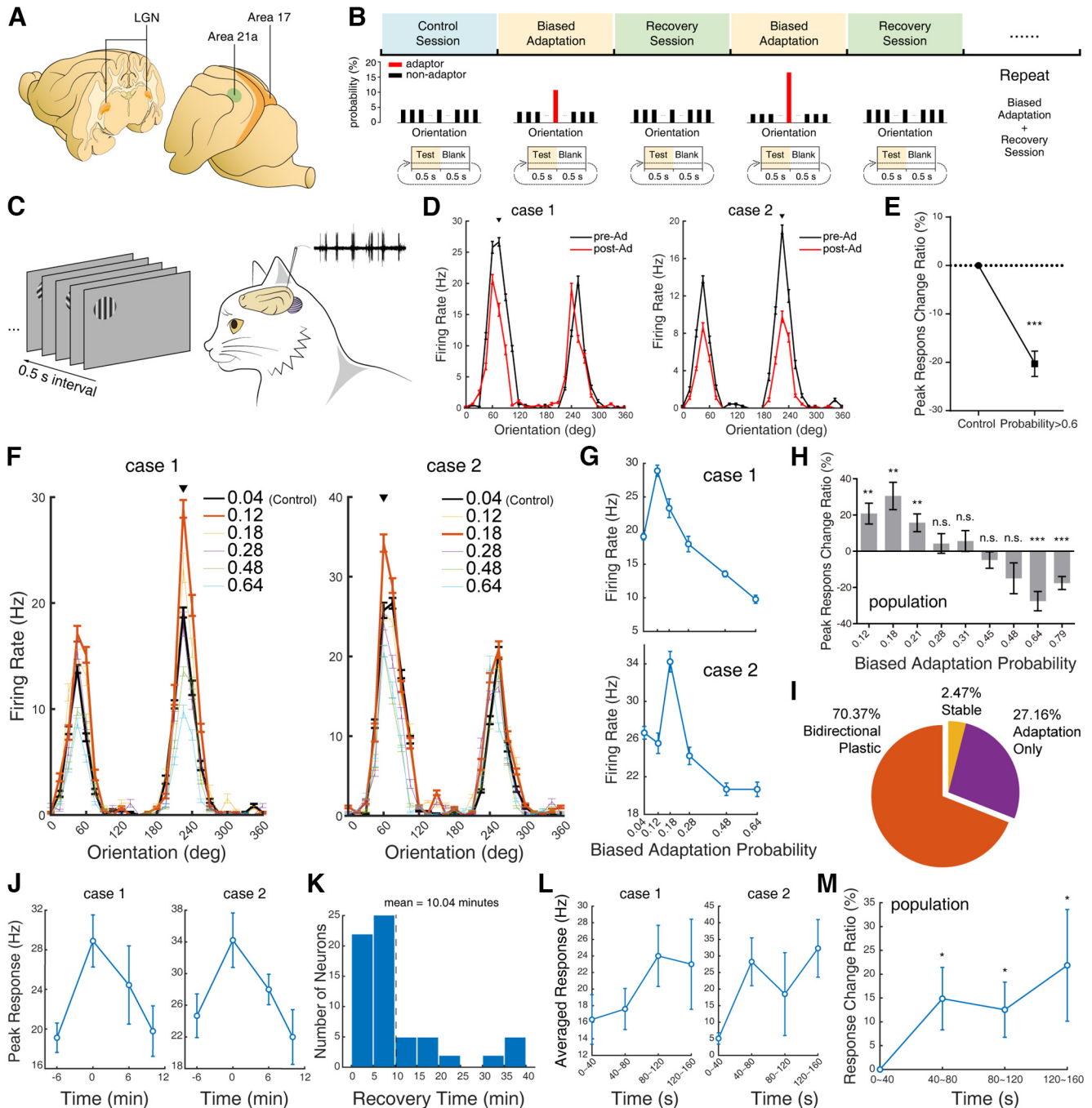


Figure 1. Biased adaptation induces short-term bidirectional-plasticity in Area 17. **A**, Brain regions being studied in this study are LGN and Areas 17 and 21a. **B**, Schematic figure of the experimental design. Top, The temporal order of stimulation sessions; middle, the distribution of orientations during each session; and bottom, the temporal structure (test/blank) of a single stimulus. **C**, Schematic figure of stimulation and recording protocol. **D**, Orientation tuning curves of two typical neurons exposed to high-intensity (biased-adaptation probability > 0.6) biased-adaptation stimulus. Black and red lines indicate preadaptation and postadaptation conditions, respectively. Arrows indicate the orientations of adaptors. **E**, Population statistics of peak response change ratio (%) after high-intensity biased-adaptation stimulus. **F**, Orientation tuning curves of two typical cases exposed to biased-adaptation stimulation; colors of lines indicate biased-adaptation probabilities; arrows indicate the orientations of adaptors. **G**, Peak response curves of two typical cases in **F**. **H**, Population peak response change ratios of Area 17 neurons exposed to biased-adaptation stimulation. **I**, Proportion of bidirectional-plastic, adaptation-only, and stable neurons. **J**, Peak responses of two typical neurons before (-6 min), during (0 min), and after ($6, 12$ min) potentiation induction. **K**, Recovery time of potentiation-exhibiting neurons after potentiation induction. The mean recovery time is 10.04 min. **L**, Two typical cases, averaged neuronal responses to adaptors over time during biased-adaptation stimulation. **M**, Population response-change ratios of tested neuronal responses to adaptors over time during biased-adaptation stimulation. Error bars indicate SEM; *** $p < 0.001$, ** $p < 0.01$, * $p < 0.05$. n.s.: not significant ($p \geq 0.05$).

In our study, orientations of adaptors were chosen within 15° near neuronal preferred orientations drifting at optimal directions. With strong biased orientation-adaptation stimulation ($\text{BAP} > 0.6$), the orientation tuning curve of tested individual Area 17 neuron was suppressed near the adapted orientation (Fig. 1D). Statistically, tested Area 17 neurons exhibited the classical

orientation-adaptation effect (Fig. 1E; significant suppression, $-20.16 \pm 3.02\%$, $p = 3 \times 10^{-9}$, $n = 81$ from 7 cats) by strong biased-adaptation protocol ($\text{BAP} > 0.6$). These results confirmed the effectiveness of biased-adaptation protocol; it could induce reliable visual adaptation effects, which is consistent with previous reported suppressive effects of top-up orientation adaptation

(Kohn and Movshon, 2004; Patterson et al., 2013, 2014a) or biased orientation adaptation (Benucci et al., 2013).

However, at low biased-adaptation probability, we found that the tested individual Area 17 neurons exhibited response potentiation instead of suppression (compared to preadaptation). This potentiation was maximal at biased-adaptation probability 0.12 (Fig. 1F,G; case 1, from 19.11 ± 1.40 Hz at BAP 0.04 to 28.89 ± 2.50 Hz at BAP 0.12; $p = 0.003$, $n = 10$ repetitions) or 0.18 (Fig. 1F,G, case 2, from 26.67 ± 2.00 Hz at BAP 0.04 to 34.40 ± 3.40 Hz at BAP 0.18; $p = 0.065$, $n = 10$ repetitions). However, at a higher biased-adaptation probability (>0.28), this potentiation was reversed into suppression, and the suppression effect was enhanced as the biased-adaptation probability increased to 0.64 (Fig. 1F,G; case 1, from 19.11 ± 1.40 Hz at BAP 0.04 to 9.78 ± 1.80 Hz at BAP 0.64, $p = 0.001$; case 2, from 26.67 ± 2.00 Hz at BAP 0.04 to 20.89 ± 2.40 Hz at BAP 0.64, $p = 0.083$; $n = 10$ repetitions). Population statistics of neurons from seven cats showed identical results (Fig. 1H); in Area 17, low-intensity of biased-adaptation could induce neuronal response potentiation (BAP 0.12, $20.83 \pm 5.77\%$, $p = 0.002$, $n = 25$; BAP 0.18, $30.54 \pm 7.59\%$, $p = 0.001$, $n = 27$; BAP 0.21, $15.74 \pm 4.91\%$, $p = 0.004$, $n = 61$), whereas high intensity could induce significant suppression (BAP 0.64, $-27.56 \pm 5.34\%$, $p = 2 \times 10^{-4}$, $n = 21$; BAP 0.79, $-17.57 \pm 3.59\%$, $p = 7 \times 10^{-5}$, $n = 60$). The difference in sampled neuron numbers was because of slightly different protocols (12 and 24 directions would result in different BAPs) and an incomplete dataset because of strict objective criteria including stable single-unit recording, full recovery from previous biased-adaptation probability, and so on (see above, Materials and Methods). It is notable that a full set of biased-adaptation recordings lasted at least 100 min (including recovery time after each BAP session), and an incomplete dataset of a particular neuron was not rare.

This biphasic form of the adaptation effect (that the same neuron could significantly exhibit potentiation under low BAP and suppression under high BAP) is distinct from the classical suppressive-only visual adaptation effect (Kohn, 2007; Webster, 2015), and we named this novel adaptation effect bidirectional plasticity. For each individual neuron, when it shows statistically significant potentiation at at least one low BAP and suppression at at least one high BAP, we define it as bidirectional plastic. Overall, a majority (70.37%, 57/81) of Area 17 neurons exhibited bidirectional-plasticity, and only a minority (27.16%, 22/81) of Area 17 neurons exhibited pure response suppression after biased adaptation (Fig. 1I).

It is notable that for low BAP (such as 0.21 and 0.07 for nonadaptors), 10 repetitions of 12 directions only took 140 s to finish, which means within 140 s the neuronal response to the adapted orientation could be significantly enhanced, suggesting a rapid inducing time. To quantify the recovery time of this bidirectional-plasticity, after the induction by biased-adaptation protocol, we successively stimulated and recorded bidirectional-plastic neurons with the Control stimulus (each lasting for 2 ~ 3 min). Tested neurons were considered recovered once their peak responses were not significantly different from the preadaptation response level (Fig. 1J). For tested potentiation-exhibiting neurons ($n = 72$), the averaged recovery time of potentiation or suppression was 10.04 ± 1.11 min (Fig. 1K) or 14.23 ± 1.50 min, respectively. The results above suggest that this bidirectional-plasticity is a short-term effect.

To further investigate the detailed inducing timeline of potentiation effect during biased-adaptation stimulation, we examined the dynamics of neuronal responses to adaptors. For data of

BAP ≤ 0.21 (which could induce potentiation effect; Fig. 1H), we averaged the neuronal responses to adaptors at fixed intervals (40 s) to check whether there existed a stable tendency of response change. We found that tested neuronal responses to adaptors exhibited a potentiation trend over time (Fig. 1L); during the biased-adaptation stimulation, compared with initial state (0 ~ 40 s from stimulus onset), the tested neuronal responses to adaptors exhibited a potentiation trend from 40 s to 160 s after stimulus onset, suggesting a rapid potentiation effect. At the population level, we also found that tested neurons could exhibit potentiation during 40 ~ 160 s from stimulus-onset (Fig. 1M); tested neurons exhibited significant potentiation during 40 ~ 80 s ($14.86 \pm 6.60\%$, $p = 0.026$, $n = 72$), 80 ~ 120 s ($12.55 \pm 5.83\%$, $p = 0.026$, $n = 72$), and 120 ~ 160 s ($21.9 \pm 11.8\%$, $p = 0.034$, $n = 72$). The above results suggested that the potentiation effect could be induced within dozens of seconds, showing a rapid modulation of neuronal response.

We also examined the potential influence of the probability of nonadaptors on bidirectional-plasticity and found that tested neurons could exhibit bidirectional-plasticity using 12 and 24 directions, and there was little difference between the BAPs corresponding to maximal neuronal potentiation. These results suggested that the influence of the probability of nonadaptors on bidirectional-plasticity was limited.

Potentiation induced by biased-adaptation in Area 17 is feature selective but interocular transferable

Feature-preference modulation during adaptation may reflect the interactions between feature-coding channels in visual system (Maffei et al., 1973; Movshon and Lennie, 1979; Carandini et al., 1998; Müller et al., 1999; Dragoi et al., 2002; Felsen et al., 2002; Solomon and Kohn, 2014), suggesting cortical circuit mechanisms. To further investigate the potential mechanisms of potentiation of Area 17 neurons induced by the biased-adaptation protocol, we studied two aspects of neuronal response change in Area 17, inducing and transferring stages. We used 12 directions for stimulation in these experiments (BAP of Control stimulus was 0.08).

During the inducing stage (when biased-adaptation protocol was applied), the above findings have suggested that majority of Area 17 neurons could exhibit potentiation under optimal pattern parameters (Fig. 1H). However, when nonoptimal (nonpreferred) pattern parameters (50 or 150% preferred spatial-frequency, or 50% contrast) were chosen in biased-adaptation protocol, it could not induce a potentiation effect (Fig. 2A). Population statistics of neurons from two cats suggest an identical result (Fig. 2B); when biased-adaptation probability is <0.32 , under 50% preferred spatial-frequency (group SF−), 150% preferred spatial-frequency (group SF+), and 50% contrast (group C−) conditions, tested potentiation-exhibiting neurons (significantly potentiated when induced by optimal condition; SF−, $20.51 \pm 5.11\%$, $p = 0.001$, $n = 17$; SF+, $25.71 \pm 5.90\%$, $p = 8 \times 10^{-4}$, $n = 14$; C−, $22.43 \pm 5.01\%$, $p = 5 \times 10^{-4}$, $n = 15$) were significantly suppressed under each nonoptimal condition (SF−, $-5.63 \pm 1.62\%$, $p = 0.002$, $n = 17$; SF+, $-24.65 \pm 6.50\%$, $p = 0.001$, $n = 14$; C−, $-8.31 \pm 2.33\%$, $p = 0.002$, $n = 15$). Moreover, when biased-adaptation probability equaled 0.45, tested neurons did not exhibit a significant response change under optimal condition (Fig. 2C; SF−, $4.12 \pm 4.35\%$, $p = 0.357$, $n = 17$; SF+, $-1.25 \pm 5.42\%$, $p = 0.822$, $n = 14$; C−, $4.20 \pm 3.39\%$, $p = 0.236$, $n = 15$) and were significantly suppressed under nonoptimal conditions (SF−, $-12.05 \pm 4.90\%$, $p = 0.013$, $n = 17$;

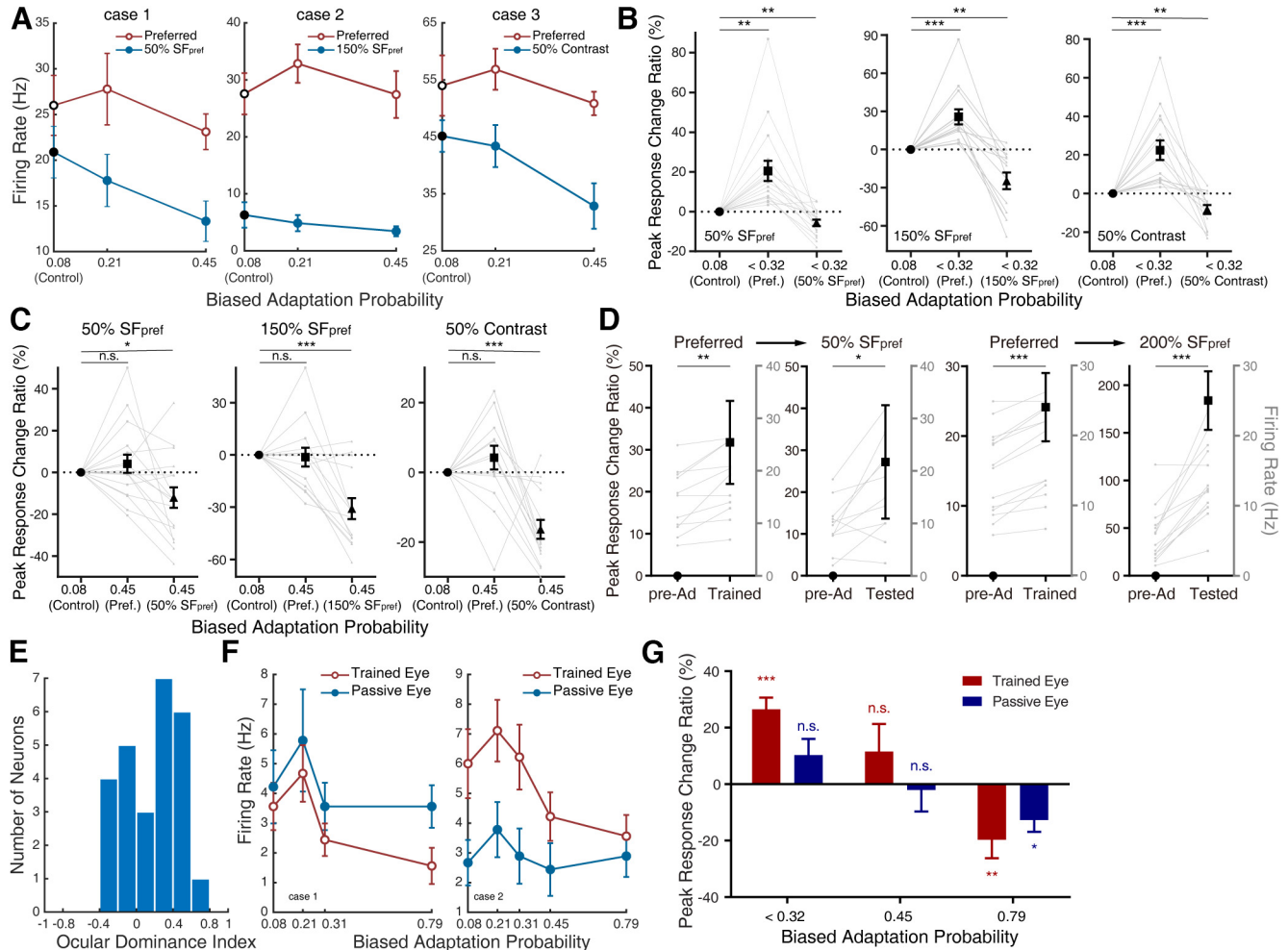


Figure 2. Potentiation induced by biased adaptation in Area 17 is selectively induced by optimal stimuli but interocularly transferable. **A**, The induction of bidirectional plasticity in three typical neurons exposed to preferred and nonpreferred stimuli. Case 1, 50% preferred spatial frequency; case 2, 150% preferred spatial frequency; case 3, 50% contrast. Red lines (open circle) are induced by preferred stimuli, whereas blue lines (solid circle) are induced by nonpreferred stimuli. Black circles indicate Control condition. **B**, Population and individual peak response change ratios of Area 17 neurons exposed to preferred and nonpreferred stimuli (biased-adaptation probability < 0.32). Black points indicate population statistical results, whereas gray points indicate individual data. **C**, Same as **B**, when biased-adaptation probability equals 0.45. **D**, Population statistics of peak response change ratios during transferring period. Neurons were initially exposed to Control stimulus using preferred or nonpreferred (50 or 200% SF_{pref}) parameters (pre-Ad); then neurons were potentiated by biased-adaptation stimulus using preferred parameters (Trained under Preferred condition). After potentiation induction, neurons were immediately exposed to Control stimulation using nonpreferred parameters (Tested under non-preferred condition, peak response change ratios were calculated based on pre-Ad using corresponding nonpreferred parameters.). Black Points indicate population peak response change ratios, and gray points indicate individual neuronal firing rates. **E**, Histogram of Ocular Dominance Index ($n = 26$) of Area 17 neurons; 1 means purely contralateral driven, -1 means purely ipsilateral driven. **F**, Peak response curves of two typical neurons in interocular transfer experiment. Red lines (open circle) are evoked by Trained Eye (which is monocularly induced), and blue lines (solid circle) are evoked by Passive Eye (which is covered during induction and tested after monocular induction). **G**, Population peak response change ratios of potentiation-exhibiting Area 17 neurons. Red bars indicate the Trained Eye, whereas blue bars indicate the Passive Eye. Error bars indicate SEM; *** $p < 0.001$, ** $p < 0.01$, * $p < 0.05$. It is notable that we adopted the 12-directions protocol in these experiments, and thus the probability of the Control stimulus was 0.08 instead of 0.04. pre-Ad: preadaptation. n.s.: not significant ($p \geq 0.05$).

SF+, $-30.86 \pm 6.02\%$, $p = 2 \times 10^{-4}$, $n = 14$; C-, $-16.36 \pm 2.73\%$, $p = 3 \times 10^{-5}$, $n = 15$). This result suggests that potentiation could only be induced at around neuronal preferred pattern-parameter condition. In other words, the potentiation induced by biased-adaptation protocol is pattern-feature selective.

During the transferring stage (after the potentiation effect was already induced by optimal stimuli), we investigated whether the potentiation induced by optimal stimuli remained under nonoptimal pattern condition. In other words, we examined whether the potentiation of Area 17 neurons could be transferred between different pattern-feature conditions. We induced potentiation in Area 17 neurons with proper biased-adaptation probability under optimal pattern parameters and then immediately stimulated these neurons under Control

conditions using nonoptimal parameters (50 or 200% preferred spatial frequency). Peak response change ratios were calculated based on corresponding preadaptation Control (optimal or nonoptimal) results.

Consistent with previous results, tested neurons (from two cats) exhibited significant potentiation after biased-adaptation stimulation under optimal parameters (Fig. 2D; Trained, 50% SF_{pref} Group, $31.75 \pm 9.90\%$, $p = 0.005$, $n = 11$; 200% SF_{pref} Group, $24.14 \pm 4.89\%$, $p = 3 \times 10^{-4}$, $n = 14$). However, when exposed to nonoptimal parameters immediately afterward, tested neurons still exhibited significant potentiation relative to corresponding preadaptation Control (nonoptimal) results (Fig. 2D; Tested, 50% SF_{pref} Group, $27.20 \pm 13.60\%$, $p = 0.036$, $n = 11$; 200% SF_{pref} Group, $184.00 \pm 30.80\%$, $p = 5 \times 10^{-5}$, $n = 14$, large peak response change ratios were because of poor activation of

tested neurons under 200% SF_{pref} conditions before biased adaptation). Similarly, when potentiation-exhibiting Area 17 neurons were exposed to optimal Control stimulus (with identical duration to nonoptimal Control stimulus) immediately after potentiation induction, their response potentiation could also remain ($10.65 \pm 3.42\%$, $p = 0.001$, $n = 72$ from 7 cats). These results suggest that the potentiation effect could be transferred from optimal pattern condition to nonoptimal pattern condition. It is notable that according to the previous literature (Saul and Cynader, 1989), the suppressive orientation-adaptation effect is transferable over a broad range of spatial frequency (at least ± 2 octaves from preferred spatial frequency), and the transferable potentiation effect in our result (± 1 octave from preferred spatial frequency) is similar to that in the previous literature.

In addition to spatial frequency, eye preference was also examined. Previous literature has shown that the orientation-adaptation effect could transfer interocularly in cat Areas 17 and 18 (Maffei et al., 1986). Considering that neurons in Areas 17 and 18 are mainly binocularly driven (Hubel and Wiesel, 1962; Maffei et al., 1986; Kasamatsu and Imamura, 2020), whereas LGN neurons are monocularly driven (Sanderson, 1971; LeVay and Ferster, 1977; Weyand, 2016; Ghodrati et al., 2017), interocular transferability supports the cortical origin hypothesis of orientation adaptation.

To investigate the origin (cortex or subcortex) of potentiation, we then examined its interocular transferability. The ODI of tested Area 17 neurons is 0.15 ± 0.06 (Fig. 2E; $n = 26$), consistent with previous studies (Hubel and Wiesel, 1962; Wiesel and Hubel, 1963; Kara and Boyd, 2009; Kasamatsu and Imamura, 2020) showing a binocular-driven feature. The interocular transferability test consists of several steps. First, we separately recorded preadaptation Area 17 neuronal responses of each eye (with the other eye covered) using Control stimulus. Second, we recorded neuronal response of the Trained Eye to biased-adaptation stimulus (Passive Eye covered). Third, we immediately recorded neuronal response of the Passive Eye to Control stimulus (Trained Eye covered). In this way, we examined the possibility that the biased-adaptation aftereffect on Area 17 neurons could be induced by one eye and be exhibited by the other eye.

As expected, we successfully reproduced potentiation of individual Area 17 neurons by solely stimulating the Trained Eye with biased adaptation (biased-adaptation probability = 0.21). More interestingly, the responses of these tested neurons driven by the Passive Eye (which only received Control stimuli) also exhibited potentiation (Fig. 2F). Population statistics of potentiation-exhibiting neurons (18/26 neurons) showed that (Fig. 2G) when biased-adaptation probability was <0.32 , neuronal responses to the Trained Eye and the Passive Eye both exhibited potentiation (Trained Eye, $26.48 \pm 4.14\%$, $p = 2 \times 10^{-5}$, $n = 18$; Passive Eye, $10.33 \pm 5.73\%$, $p = 0.0675$, $n = 18$) significantly or nonsignificantly; when biased-adaptation probability equaled 0.79, neuronal responses to the Trained Eye and the Passive Eye were both significantly suppressed (Trained Eye, $-19.68 \pm 6.53\%$, $p = 0.006$, $n = 18$; Passive Eye, $-12.67 \pm 4.25\%$, $p = 0.015$, $n = 16$; tests of two neurons were skipped because of unsuccessful recovery; see above, Materials and Methods). Proportion analysis showed that among tested potentiation-exhibiting neurons, 72.22% (13/18 neurons) could exhibit significant potentiation when exposed to the Passive Eye. We noticed that when BAP was <0.32 , tested neuronal responses to the Passive Eye exhibited nonsignificant potentiation. This was because of the large variation caused by a few (11.11%, 2/18) strongly suppressed neurons (whose peak response change

ratios were less than -20%). The above results suggested the overall interocular transferability of potentiation effect.

Moreover, there is no significant difference in ODI between interocular transferable and the rest of the neurons ($ODI_{transferable} = 0.225 \pm 0.082$, $ODI_{rest} = 0.084 \pm 0.092$; $p = 0.264$, two-sample Student's *t* test; $n_{transferable} = 13$, $n_{rest} = 13$).

The above results suggest that the potentiation of Area 17 neurons induced by biased-adaptation protocol might originate within primary visual cortex rather than LGN. To examine this idea, we next performed latency analysis.

Bidirectional plasticity arises from the antagonistic competition of adaptation of the receptive-field

Response-latency analysis reflects the primary origin of neural inputs and has been extensively applied (Nowak et al., 1995; Angelucci and Bullier, 2003; Patterson et al., 2013; Yao et al., 2015). Neurons in Area 17 primarily receive inputs from three origins, the excitatory feedforward projections from subcortical (mainly LGN) regions, the inhibitory or excitatory horizontal connections from local cortical circuits, and the excitatory feedback projections from higher visual cortices such as Area 21a (Huang et al., 2004; Tong et al., 2011). Their effects are mainly reflected within corresponding response-latency time window; neural responses corresponding to feedforward, horizontal, and feedback inputs are primarily reflected in the early (50 ~ 100 ms), middle (100 ~ 200 ms), and late (>200 ms) epoch components from stimulus onset, respectively (Nowak et al., 1995; Angelucci and Bullier, 2003; Bair et al., 2003; Xing et al., 2011; Henry et al., 2013; Patterson et al., 2013; Shapley and Xing, 2013; Yao et al., 2015). Therefore, in this study, we examined how neural peak responses change with biased-adaptation probabilities during early (50 ~ 100 ms), middle (100 ~ 200 ms), and late (200 ~ 500 ms) epochs. Considering the potential response-latency variation and considerable proportion of slow responsive (latency >100 ms) neurons (Raiguel et al., 1989; Nowak et al., 1995), during each epoch, nonresponsive neurons were identified as outliers and were excluded (see above, Materials and Method).

We found that after biased-adaptation, neurons in Area 17 behaved differently during early, middle, and late epochs. During the early epoch (Fig. 3A), population statistics of analyzed neurons did not exhibit significant response change at BAP $0.12 \sim 0.45$ (BAP 0.12, $20.60 \pm 34.60\%$, $p = 0.759$, $n = 9$; BAP 0.18, $-30.80 \pm 20.50\%$, $p = 0.352$, $n = 8$; BAP 0.21, $3.30 \pm 14.50\%$, $p = 0.938$, $n = 21$; BAP 0.28, $-38.50 \pm 14.10\%$, $p = 0.061$, $n = 10$; BAP 0.31, $0.30 \pm 19.00\%$, $p = 0.989$, $n = 21$; BAP 0.45, $-10.70 \pm 17.60\%$, $p = 0.759$, $n = 23$) but only showed significant suppression at 0.48 and >0.6 (BAP 0.48, $-63.80 \pm 10.10\%$, $p = 8 \times 10^{-4}$, $n = 10$; BAP >0.6 , $-38.87 \pm 9.85\%$, $p = 0.004$, $n = 22$).

During the middle-epoch (Fig. 3B), population statistics of analyzed neurons exhibited slight potentiation (not significant) at BAP 0.12 (BAP 0.12, $70.10 \pm 29.90\%$, $p = 0.077$, $n = 22$) and significant potentiation at BAP $0.18 \sim 0.21$ (BAP 0.18, $92.70 \pm 33.90\%$, $p = 0.048$, $n = 23$; BAP 0.21, $42.90 \pm 15.20\%$, $p = 0.048$, $n = 29$) but did not exhibit significant response change when BAP ≥ 0.28 (BAP 0.28, $10.90 \pm 21.50\%$, $p = 0.661$, $n = 22$; BAP 0.31, $8.54 \pm 7.68\%$, $p = 0.521$, $n = 33$; BAP 0.45, $8.67 \pm 9.98\%$, $p = 0.521$, $n = 45$; BAP 0.48, $-12.40 \pm 13.90\%$, $p = 0.521$, $n = 21$; BAP >0.6 , $-5.60 \pm 12.60\%$, $p = 0.661$, $n = 50$).

During the late-epoch (Fig. 3C), population statistics of analyzed neurons exhibited slight potentiation (not significant) at BAP 0.12 ($26.30 \pm 14.30\%$, $p = 0.090$, $n = 24$) and significant

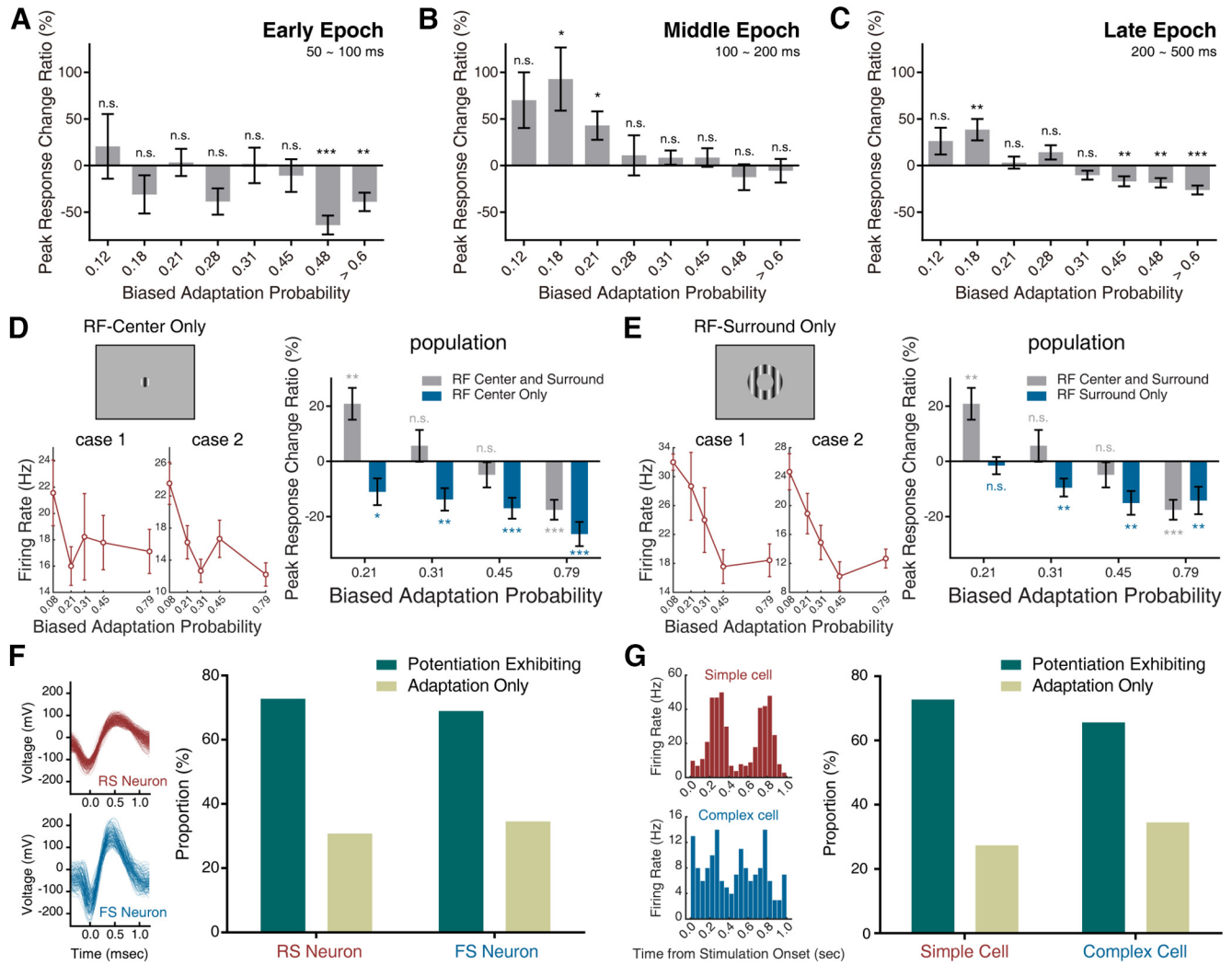


Figure 3. Latency analysis and RF structure dependence of bidirectional-plasticity in Area 17. **A**, Population peak response change ratios of tested Area 17 neurons during the early epoch of biased-adaptation stimulation. **B**, Population peak response change ratios of tested Area 17 neurons during the middle epoch of biased-adaptation stimulation. **C**, Population peak response change ratios of tested Area 17 neurons during the late epoch of biased-adaptation stimulation. **D**, Peak response (change) ratios of Area 17 neurons exposed to RF-center-only (1.5–2.5° in diameter) stimulation. Top left, Schematic diagram of stimulation field. Bottom left, Peak response curves of two typical neurons. Right, Population peak response change ratios of Area 17 neurons. Blue bars indicate RF-center-only condition, whereas the gray bars are from both RF center and surround (adopted from Fig. 1H). **E**, same with **D**, under RF-surround-only condition (annular, 4° internal and 10° external in diameter). Blue bars in right figure indicate RF-surround-only condition. Error bars indicate SEM. **F**, RS/FS classification analysis. Left, PSTH examples of RS/FS neurons. Right, Proportions of potentiation-exhibiting or adaptation-only neurons among RS ($n = 54$)/FS ($n = 51$) neurons. **G**, Simple/Complex classification analysis. Left, PSTH examples of Simple/Complex cells. Right, Proportions of potentiation-exhibiting or adaptation-only neurons among Simple ($n = 44$)/Complex ($n = 61$) cells; *** $p < 0.001$, ** $p < 0.01$, * $p < 0.05$. n.s.: not significant ($p \geq 0.05$).

potentiation at BAP 0.18 ($38.50 \pm 11.50\%$, $p = 0.008$, $n = 24$); these neurons showed no significant response change at BAP 0.21 ~ 0.31 (BAP 0.21, $3.19 \pm 6.49\%$, $p = 0.626$, $n = 31$; BAP 0.28, $14.20 \pm 7.60\%$, $p = 0.090$, $n = 24$; BAP 0.31, $-10.32 \pm 4.75\%$, $p = 0.059$, $n = 35$) and were significantly suppressed when BAP ≥ 0.45 (BAP 0.45, $-16.83 \pm 5.42\%$, $p = 0.008$, $n = 34$; BAP 0.48, $-18.36 \pm 4.98\%$, $p = 0.004$, $n = 23$; BAP > 0.6 , $-26.14 \pm 4.74\%$, $p = 2 \times 10^{-6}$, $n = 53$). The proportions of potentiation-exhibiting neurons (among responsive neurons) when BAP < 0.32 during early, middle, and late epochs are 47.22, 64.62, and 58.82%, respectively.

The results above showed that the potentiation effect seemed to appear in the middle epoch, in which the intracortical horizontal connections started to play major role. As a previous study suggested, horizontal connections drive major neural responses of RF extended surround (Li and Li, 1994; Li et al., 2001; Angelucci et al., 2017; Wang et al., 2020). Thus, we next

examined the detailed receptive field property of bidirectional plasticity.

Neurons in Area 17 were stimulated by the same biased-adaptation protocol under two conditions (Fig. 3D,E, top left), annular (4° internal and 10° external diameter) and small (1.5–2.5° diameter) stimulation fields. The annular or small stimulation field was designed to only cover the surround part (RF extended surround, the same below) or center part (classical RF, the same below) of neural RF, respectively (Durand et al., 2007). The biased-adaptation probability gradient was set to 0.21, 0.31, 0.45, and 0.79 to investigate the difference in bidirectional plasticity patterns under different stimulation field conditions.

We found that under small stimulation field (1.5 ~ 2.5° diameter) condition, tested individual Area 17 neurons only exhibited suppression effects (Fig. 3D, bottom left), similar to classical adaptation. Population statistics showed identical results (Fig. 3D, right); tested neurons were significantly suppressed at all

tested biased-adaptation probabilities (BAP 0.21, $-11.01 \pm 4.84\%$, $p = 0.017$; BAP 0.31, $-13.77 \pm 4.06\%$, $p = 0.004$; BAP 0.45, $-16.99 \pm 3.81\%$, $p = 6 \times 10^{-4}$; BAP 0.79, $-26.37 \pm 4.37\%$, $p = 2 \times 10^{-5}$; $n = 20$). This result is distinct from our previous findings (using large stimulation-field, 7° diameter) that Area 17 neurons exhibited bidirectional plasticity (Fig. 1*H*, and Fig. 3*D*, right, gray bars), suggesting that the inhibitory RF surround is necessary for the generation of potentiation effect induced by biased adaptation.

Next, we used annulus stimulation field to only adapt the RF surround with biased adaptation and found that tested individual neurons only exhibited a suppression effect (Fig. 3*E*, bottom left). Population statistics showed identical results (Fig. 3*E*, right); tested neurons did not exhibit significant response change at BAP 0.21 ($-1.51 \pm 3.12\%$, $p = 0.317$, $n = 22$) but were significantly suppressed when BAP ≥ 0.31 (BAP 0.31, $-9.50 \pm 3.28\%$, $p = 0.007$; BAP 0.45, $-15.08 \pm 4.30\%$, $p = 0.004$; BAP 0.79, $-14.18 \pm 4.98\%$, $p = 0.007$; $n = 22$).

These results demonstrate that the bidirectional modulation of neural response requires the interaction of RF center and surround subareas. The bidirectional-plasticity might come from the competition of suppressive adaptation effects between RF center and antagonistic surround, reflecting the balance between inhibition and disinhibition (excitation) effects, which has been reported in traditional toping-up adaptation studies (Dragoi and Sur, 2000; Patterson et al., 2013; Solomon and Kohn, 2014).

Furthermore, we also did neuron-type (regular/fast-spiking and simple/complex; see above, Materials and Methods) classifications but found no remarkable classification specificity (Fig. 3*F,G*); proportions of potentiation-exhibiting neurons among RS and FS neurons are 70.37% (38/54) and 66.67% (34/51), respectively, and proportions of potentiation-exhibiting neurons among simple and complex neurons are 72.73% (32/44) and 65.57% (40/61), respectively.

Hierarchical propagation of bidirectional-plasticity in visual thalamo-ventral pathway

Previous works have shown that the adaptation of orientation could propagate through visual ventral pathway (Li et al., 2017). In this study, we asked in addition to Area 17, whether this bidirectional orientation adaptation effect coexists in other regions of visual system and could propagate along the visual thalamo-ventral pathway like classical orientation adaptation does. To answer this question, we conducted biased-adaptation research in LGN and Area 21a of cats.

We first stimulated LGN neurons with Control protocol, sinusoidal drifting gratings of 12 or 24 evenly distributed directions. Gratings were presented for 0.5 s with 0.5 s blank intervals. Similar to the previous literature (Daniels et al., 1977; Shou and Leventhal, 1989; Zhou et al., 1995; Ghodrati et al., 2017), LGN neurons exhibited weak orientation sensitivity (OB = 0.14 ± 0.01, $n = 71$ from two cats; see above, Materials and Methods) under cutoff spatial frequencies using mean response or FFT H1 component as criteria (see above, Materials and Methods). Then we stimulated LGN neurons with biased-adaptation protocols (12 or 24 directions, leading to two sets of BAP, see above, Materials and Methods). Adaptors were chosen at neuronal preferred orientations, and the biased-adaptation probability gradient was set from 0.28 to 0.92.

We found that tested individual LGN neurons exhibited response potentiation at BAP 0.28 ~ 0.78. This potentiation effect faded away from BAP 0.73–0.84, suggesting a further suppression trend (Fig. 4*A,B*). Population statistics of tested neurons

showed identical results (Fig. 4*C*); tested LGN neurons were nonsignificantly potentiated at BAP 0.28 ~ 0.64 (BAP 0.28, $15.00 \pm 9.41\%$, $p = 0.108$, $n = 36$; BAP 0.48, $21.30 \pm 11.10\%$, $p = 0.093$, $n = 36$; BAP 0.64, $13.85 \pm 8.09\%$, $p = 0.108$, $n = 36$), and exhibited significant potentiation at BAP 0.73 ~ 0.78 (BAP 0.73, $27.09 \pm 8.40\%$, $p = 0.009$, $n = 36$; BAP 0.78, $38.20 \pm 12.00\%$, $p = 0.009$, $n = 33$). These neurons did not exhibit significant response change at BAP 0.84 ~ 0.92 (BAP 0.84, $7.3 \pm 15.0\%$, $p = 0.632$, $n = 21$; BAP 0.85, $5.86 \pm 8.86\%$, $p = 0.577$, $n = 35$; BAP 0.88, $-7.80 \pm 11.80\%$, $p = 0.577$, $n = 35$; BAP 0.92, $-13.80 \pm 12.10\%$, $p = 0.393$, $n = 31$) but suggested the tendency of further suppression. The difference in sampled neuron numbers was because of different direction numbers used during stimulation (resulting in different BAPs), as well as objective and strict criteria (see above, Materials and Methods).

Together, we found that LGN neurons could also be bidirectional-plastic under biased-adaptation protocol but with a distinct manner comparing with cortical neurons. The switch threshold of potentiation and suppression (BAP > 0.84) is much higher than that of cortical neurons (BAP > 0.31), which is unexpected but reasonable (see below, Discussion). The proportion of potentiation-exhibiting neurons in LGN is 87.32%, higher than in Area 17 neurons (Fig. 4*D*).

Previous researches have revealed that massive (31 ~ 58%) inputs to LGN neurons are feedback projections from Area 17 (Guillery, 1969; Montero, 1991; Erişir et al., 1998; Van Horn et al., 2000). Using the latency analysis method, we attempted to examine the origin of LGN bidirectional-plasticity. Time windows were chosen based on the previous literature (Troy and Lennie, 1987; Lu et al., 1995; Guido and Sherman, 1998); the early epoch (30 ~ 80 ms) components reflect the inputs from retina and LGN interneurons, whereas the middle epoch (80 ~ 200 ms) and late epoch (200 ~ 500 ms) components mainly reflect feedback projections from Area 17 (directly or indirectly). Considering the potential response-latency variation and considerable proportion (approximately half) of slow-responsive (latency > 80 ms) LGN neurons (Troy and Lennie, 1987; Lu et al., 1995; Guido and Sherman, 1998), during each epoch, nonresponsive neurons were identified as outliers and were excluded (see above, Materials and Methods).

During the early epoch (Fig. 4*E*, left), responses of analyzed LGN neurons did not significantly changed at all tested BAPs (BAP 0.28, $9.80 \pm 16.30\%$, $p = 0.627$, $n = 20$; BAP 0.48, $25.70 \pm 21.90\%$, $p = 0.627$, $n = 20$; BAP 0.64, $16.30 \pm 17.10\%$, $p = 0.627$, $n = 20$; BAP 0.73, $30.00 \pm 26.30\%$, $p = 0.627$, $n = 20$; BAP 0.78, $17.60 \pm 19.30\%$, $p = 0.627$, $n = 19$; BAP 0.84, $11.60 \pm 18.00\%$, $p = 0.627$, $n = 13$; BAP 0.85, $-4.40 \pm 26.90\%$, $p = 0.873$, $n = 15$; BAP 0.88, $-37.70 \pm 15.10\%$, $p = 0.234$, $n = 15$; BAP 0.92, $-16.50 \pm 22.80\%$, $p = 0.627$, $n = 13$). Repeated p values were because of the false discovery rate method used for multiple comparison corrections.

During the middle epoch (Fig. 4*E*, middle), responses of analyzed LGN neurons exhibited significant potentiation at BAP 0.28 ~ 0.78 (BAP 0.28, $29.40 \pm 10.80\%$, $p = 0.014$, $n = 36$; BAP 0.48, $26.23 \pm 9.96\%$, $p = 0.014$, $n = 34$; BAP 0.64, $42.90 \pm 11.70\%$, $p = 0.007$, $n = 36$; BAP 0.73, $38.50 \pm 12.80\%$, $p = 0.009$, $n = 36$; BAP 0.78, $30.90 \pm 15.00\%$, $p = 0.043$, $n = 32$), and exhibited slight nonsignificant potentiation at BAP 0.84 ~ 0.85 (BAP 0.84, $33.20 \pm 18.80\%$, $p = 0.071$, $n = 20$; BAP 0.85, $16.80 \pm 12.30\%$, $p = 0.113$, $n = 30$). Tested neurons exhibited nonsignificant suppression at BAP 0.88 ~ 0.92 (BAP 0.88, $-12.20 \pm 12.00\%$, $p = 0.318$, $n = 30$; BAP 0.92, $-23.40 \pm 13.70\%$, $p = 0.113$, $n = 27$).

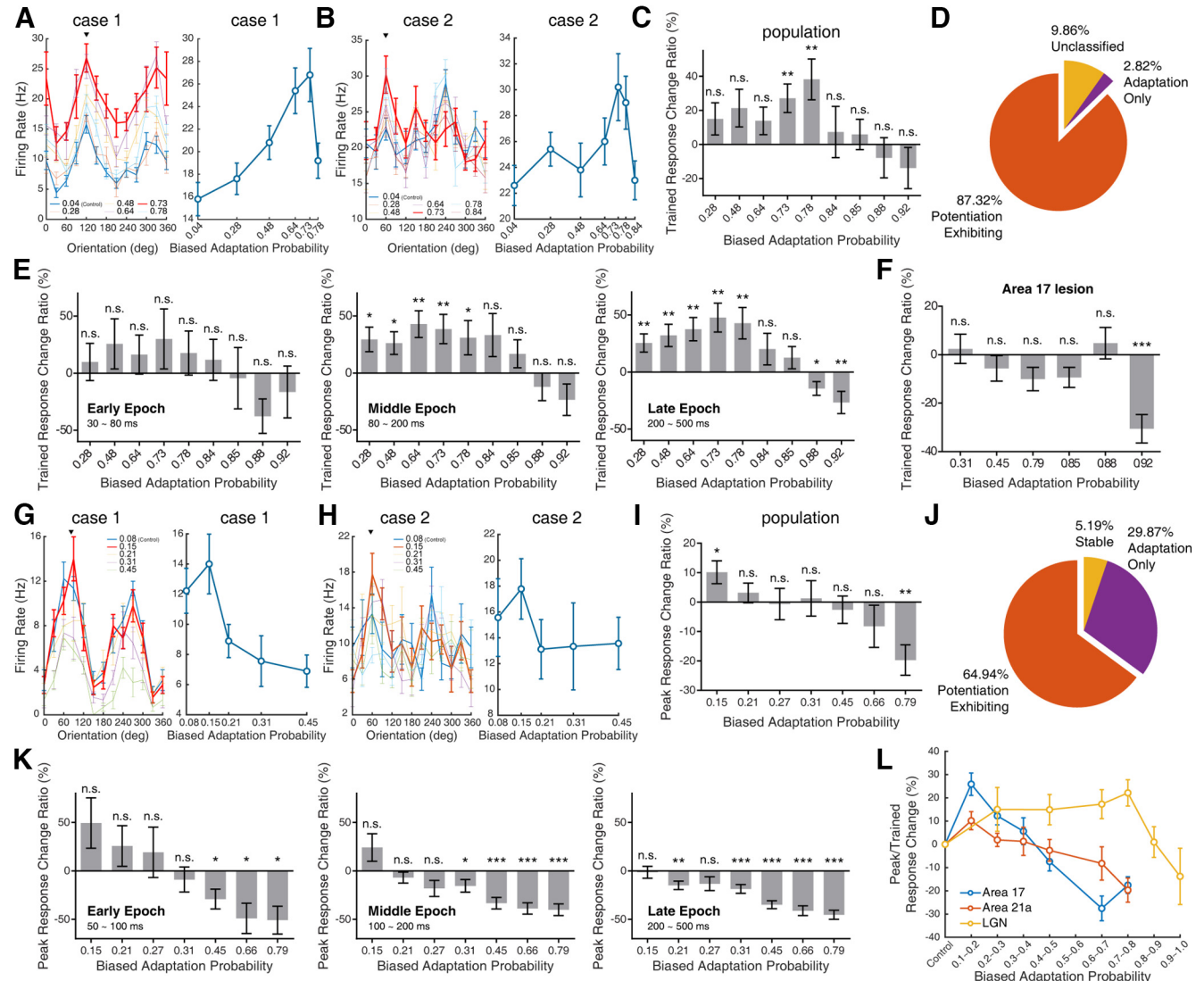


Figure 4. Bidirectional plasticity coexists in LGN and Area 21a with hierarchical progressive patterns. **A, B**, Two typical LGN neurons exposed to biased-adaptation stimulation. For each case, orientation tuning curves of two typical cases, colors of lines indicate biased-adaptation probabilities, arrows indicate the orientations of adaptors (left); trained response curves of two typical cases (right). **C**, Population trained response change ratios of LGN neurons exposed to biased-adaptation stimulation. **D**, Proportion of potentiation-exhibiting, adaptation-only, and unclassified neurons in LGN. **E**, Population trained response change ratios of tested LGN neurons during early, middle, and late epoch of biased-adaptation stimulation. **F**, Population trained response change ratios of LGN neurons with the lesion of Area 17. **G, H**, Two typical Area 21a neurons exposed to biased-adaptation stimulation. For each case, orientation tuning curves of two typical cases; colors of lines indicate biased-adaptation probabilities, and arrows indicate the orientations of adaptors (left); peak response curves of two typical cases (right). **I**, Population peak response change ratios of Area 21a neurons exposed to biased-adaptation stimulation. **J**, Proportion of potentiation-exhibiting, adaptation-only, and stable neurons in Area 21a. **K**, Population peak response change ratios of tested Area 21a neurons during early, middle, and late epoch of biased-adaptation stimulation. **L**, Population peak/trained response change ratio curves of LGN, Area 17, and Area 21a shown in one figure for comparison. Data are adopted from Figures 1H and 4, C and I. Colored lines indicate brain regions. Error bars indicate SEM; *** $p < 0.001$, ** $p < 0.01$, * $p < 0.05$. n.s.: not significant ($p \geq 0.05$).

During the late epoch (Fig. 4E, right), responses of analyzed LGN neurons exhibited significant potentiation at BAP $0.28 \sim 0.78$ (BAP 0.28, $25.40 \pm 8.01\%$, $p = 0.004$, $n = 36$; BAP 0.48, $32.14 \pm 9.74\%$, $p = 0.003$, $n = 36$; BAP 0.64, $37.50 \pm 10.20\%$, $p = 0.003$, $n = 36$; BAP 0.73, $47.70 \pm 12.70\%$, $p = 0.003$, $n = 36$; BAP 0.78, $42.80 \pm 13.80\%$, $p = 0.004$, $n = 33$). These analyzed neurons exhibited nonsignificant potentiation at BAP $0.84 \sim 0.85$ (BAP 0.84, $20.10 \pm 13.90\%$, $p = 0.091$, $n = 21$; BAP 0.85, $12.62 \pm 9.77\%$, $p = 0.102$, $n = 35$) and significant suppression at BAP $0.88 \sim 0.92$ (BAP 0.88, $-14.43 \pm 6.01\%$, $p = 0.014$, $n = 34$; BAP 0.92, $-26.66 \pm 9.82\%$, $p = 0.009$, $n = 28$).

Proportional analysis also showed a latency-related pattern; according to the same criteria in Area 17 (a neuron was considered to exhibit potentiation when its response significantly

increased after the biased-adaptation stimulation), we found in LGN, 42.86% (15/35) of responsive neurons exhibited potentiation at BAP $0.28 \sim 0.78$ during the early epoch, however 53.03% (35/66) and 66.20% (47/71) of responsive neurons exhibited potentiation at BAP $0.28 \sim 0.78$ during the middle and late epoch, respectively. We noticed that during the early epoch, although as a population tested neurons did not exhibit statistically significant potentiation in their population averaged response, individual neurons in LGN showed great divergence. A strong potentiation effect (trained response change ratio $> 100\%$) could be found in a few neurons (17.14%, 6/35), whereas the rest of neurons exhibited either suppression (-57.14% , 20/35) or moderate potentiation (25.71%, 9/35), leading to high variance of statistical results. This divergence might reflect more

complicated circuit origins in addition to cortical feedback. Considering that the superior colliculus (SC) could encode visual saliency before V1 (White et al., 2017) and project to LGN (Liu et al., 2022), it is possible that the potentiation of some LGN neurons during the early epoch might be influenced by the SC (see below, Discussion).

These latency-related findings altogether suggested that the bidirectional-plasticity property of LGN neurons might derive from the feedback projection of Area 17, consistent with our findings that bidirectional-plasticity started to appear during the middle epoch in Area 17. However, subcortical (like superior colliculus) mechanisms may also contribute to the early epoch potentiation of some LGN neurons.

To further clarify the cortical origin hypothesis, we inactivated Area 17 with liquid nitrogen (see above, Materials and Methods) to remove cortical feedback and then examined the effect of biased adaptation in LGN neurons. We set the BAP gradient ($0.31 \sim 0.92$) and found that after cortical lesion, distinct from previous experimental results (Fig. 4C), tested LGN neurons did not exhibit potentiation effect but only showed adaptive suppression (Fig. 4F). Population statistics showed that tested neurons did not exhibit a significant response change at BAP 0.31, 0.45 or 0.88 (BAP 0.31, $2.44 \pm 6.04\%$, $p = 0.692$; BAP 0.45, $-5.61 \pm 5.29\%$, $p = 0.461$; BAP 0.88, $4.78 \pm 6.48\%$, $p = 0.568$; $n = 15$) but showed slight suppression (not significant) at BAP 0.79 ~ 0.85 (BAP 0.79, $-10.02 \pm 4.86\%$, $p = 0.058$; BAP 0.85, $-9.35 \pm 4.12\%$, $p = 0.058$; $n = 15$) and significant suppression at BAP 0.92 ($-30.55 \pm 5.89\%$, $p = 6 \times 10^{-4}$, $n = 15$). This lesion experiment demonstrates that the bidirectional-plasticity in LGN might be derived from the feedback projection of Area 17.

In Area 21a we first recorded neurons with Control protocol, sinusoidal drifting gratings of 12 evenly distributed directions. Gratings were presented for 0.5 s with 0.5 s blank intervals. Comparing them with Area 17 neurons, Area 21a neurons also exhibited strong orientation selectivity ($OSI = 0.40 \pm 0.03$, $n = 77$), and the average preferred spatial frequency is lower [0.37 cycle per degree (cpd), $n = 77$] than Area 17 (1.08 cpd, $n = 105$). These properties of recorded neurons in Area 21a are consistent with the previous literature (Dreher et al., 1993; Morley and Vickery, 1997).

Next, we stimulated Area 21a neurons with biased-adaptation protocol (biased-adaptation probability gradient $0.15 \sim 0.79$; a finer BAP gradient was used during the second half of the experiment, leading to different neuron numbers; see above, Materials and Methods) and found the bidirectional-plasticity feature in tested individual neurons (Fig. 4G,H). Population statistics showed identical results (Fig. 4I); tested Area 21a neurons exhibited significant potentiation at BAP 0.15 ($10.16 \pm 3.88\%$, $p = 0.045$, $n = 37$) and were significantly suppressed at BAP 0.79 ($-19.71 \pm 5.20\%$, $p = 0.007$, $n = 30$); tested Area 21a neurons did not exhibit significant response change at BAP $0.21 \sim 0.66$ (BAP 0.21, $3.13 \pm 3.35\%$, $p = 0.618$, $n = 77$; BAP 0.27, $-0.67 \pm 5.32\%$, $p = 0.901$, $n = 37$; BAP 0.31, $1.27 \pm 6.04\%$, $p = 0.901$, $n = 73$; BAP 0.45, $-2.60 \pm 4.67\%$, $p = 0.811$, $n = 65$; BAP 0.66, $-8.23 \pm 7.15\%$, $p = 0.600$, $n = 39$) but suggested the tendency that higher adaptation intensity would induce stronger suppression. Proportion analysis showed that majority of Area 21a neurons (64.94%, 50/77) exhibited potentiation after exposed to biased-adaptation stimulation (Fig. 4J).

Latency analysis of Area 21a neurons was performed to examine the potential origin of Area 21a neuronal bidirectional-plasticity. Responses of analyzed Area 21a neurons during biased adaptation were separated into three epoch components

suggested by previous reports (Lee et al., 2007; Sundberg et al., 2012), the early epoch ($50 \sim 100$ ms), the middle epoch ($100 \sim 200$ ms), and the late epoch ($200 \sim 500$ ms). Considering the potential response-latency variation and considerable proportion of slow-responsive (latency > 100 ms) Area 21a neurons (Lee et al., 2007; Sundberg et al., 2012), during each epoch nonresponsive neurons were identified as outliers and excluded.

During the early epoch (Fig. 4K, left), population statistics of analyzed neurons showed nonsignificant potentiation at BAP $0.15 \sim 0.27$ (BAP 0.15, $49.40 \pm 26.00\%$, $p = 0.128$, $n = 20$; BAP 0.21, $25.70 \pm 21.00\%$, $p = 0.319$, $n = 40$; BAP 0.27, $19.20 \pm 26.00\%$, $p = 0.493$, $n = 20$). These neurons did not exhibit a significant response change at BAP 0.31 ($-8.90 \pm 12.90\%$, $p = 0.493$, $n = 35$). Moreover, these neurons exhibited significant suppression at BAP $0.45 \sim 0.79$ (BAP 0.45, $-29.10 \pm 10.20\%$, $p = 0.019$, $n = 36$; BAP 0.66, $-49.00 \pm 15.70\%$, $p = 0.019$, $n = 20$; BAP 0.79, $-50.80 \pm 14.40\%$, $p = 0.014$, $n = 19$).

During the middle epoch (Fig. 4K, middle), population statistics of analyzed neurons showed nonsignificant potentiation at BAP 0.15 ($24.20 \pm 14.20\%$, $p = 0.117$, $n = 27$). These analyzed neurons did not exhibit a significant response change at BAP $0.21 \sim 0.27$ (BAP 0.21, $-6.88 \pm 5.64\%$, $p = 0.228$, $n = 54$; BAP 0.27, $-18.06 \pm 8.25\%$, $p = 0.053$, $n = 27$) and exhibited significant suppression at BAP $0.31 \sim 0.79$ (BAP 0.31, $-15.39 \pm 6.58\%$, $p = 0.042$, $n = 48$; BAP 0.45, $-33.32 \pm 5.85\%$, $p = 2 \times 10^{-6}$, $n = 47$; BAP 0.66, $-38.65 \pm 5.88\%$, $p = 2 \times 10^{-6}$, $n = 26$; BAP 0.79, $-40.02 \pm 6.01\%$, $p = 2 \times 10^{-6}$, $n = 25$).

During the late epoch (Fig. 4K, right), population statistics of analyzed neurons showed no significant response change at BAP 0.15 ($-1.44 \pm 6.09\%$, $p = 0.815$, $n = 22$) as well as nonsignificant suppression at BAP 0.27 ($-13.21 \pm 7.10\%$, $p = 0.091$, $n = 21$). However, these analyzed neurons exhibited significant suppression at BAP 0.21 and $0.31 \sim 0.79$ (BAP 0.21, $-14.92 \pm 4.38\%$, $p = 0.001$, $n = 46$; BAP 0.31, $-18.59 \pm 4.52\%$, $p = 4 \times 10^{-4}$, $n = 44$; BAP 0.45, $-34.87 \pm 4.05\%$, $p = 2 \times 10^{-9}$, $n = 37$; BAP 0.66, $-41.06 \pm 5.06\%$, $p = 5 \times 10^{-7}$, $n = 26$; BAP 0.79, $-45.23 \pm 4.68\%$, $p = 4 \times 10^{-9}$, $n = 24$).

Together, the above results showed that (1) the suppression effect at high adaptation intensity could be found during all three epochs, (2) a nonsignificant potentiation effect could be found during the early and middle epochs, and (3) the extent of suppression was stronger during the middle and late epochs. Moreover, proportions of potentiation-exhibiting neurons (among responsive Area 21a neurons) at BAP $0.15 \sim 0.21$ during early, middle, and late epochs are 40.00, 46.30, and 39.58%, respectively. We noticed that during early and middle epochs, the potentiation effects of analyzed neurons are nonsignificant at BAP 0.15. This might result from the inconsistency of neuronal adaptation effects; at BAP 0.15, 35.00 and 29.63% of sampled neurons exhibited suppression during early and middle epoch, respectively. This inconsistency leads to high variance of statistical results, and these results suggest the inconsistency and complexity of Area 21a neuronal effects of biased adaptation.

The bidirectional-plasticity pattern in Area 17 and Area 21a are slightly different. Area 21a neurons have a disposition to exhibit potentiation at lower BAPs than Area 17 neurons; according to population statistics, at BAP 0.21, Area 21a neurons could not exhibit significant response change (Fig. 4I), whereas Area 17 neurons could exhibit significant potentiation (Fig. 1H). This result suggested that compared with Area 17 neurons, potentiation of Area 21a neurons requires lower biased-adaptation intensity.

The latency-analysis results of LGN and Areas 17 and 21a neurons also suggested an interesting tendency (Figs. 3A,B,C, 4E, K). Although during the early epoch, the response change patterns of neurons in LGN and Areas 17 and 21a were noisy, there was still a noticeable hierarchical trend during the middle and late epochs; from LGN to Area 21a, the potentiation effect gradually diminished, and the suppression effect was enhanced. During the middle epoch, the maximal significant potentiation inducing BAP was 0.78 for LGN and 0.21 for Area 17, whereas there was only nonsignificant potentiation at BAP 0.15 for Area 21a; during the late epoch, the minimal significant suppression inducing BAP was 0.88 for LGN, 0.45 for Area 17, and 0.21 for Area 21a.

In summary, our findings demonstrate universally existing bidirectional-plasticity along the visual thalamo–ventral pathway, with progressive hierarchical propagation pattern. The bidirectional-plasticity properties of LGN and Areas 17 and 21a neurons show a progressively changing pattern (Fig. 4L). The BAPs required for inducing potentiation and suppression are lower for neurons of higher visual areas. Moreover, the proportion of potentiation-exhibiting neurons in tested LGN, Area 17, and Area 21a neurons are 87, 70, and 65%, respectively. Together, we found that bidirectional-plasticity induced by biased adaptation exists in LGN, Area 17, and Area 21a with progressive pattern changes.

Modeling of the origin and functional significance of bidirectional-plasticity

As shown in our above experimental RF-structure data, biased-adaptations suppress (adapt) both the neural response to RF center (classical RF, the same below) and the one to surround (RF extended surround, the same below) subareas. We hypothesized that suppression of the RF excitatory center leads to inhibition of neural responses, whereas suppression of the RF inhibitory surround leads to disinhibition (excitation). The balance between excitation and inhibition can be reversed as the biased-adaptation strength increases, thus causing bidirectional-plasticity of overall neuronal response. Modeling of this RF center-surround adaptation-competition was thus performed (see above, Materials and Methods) to quantitatively simulate this effect.

Receptive-field adaptation competition model

The computing simulation model is modified from the classical DoG model (Marr and Hildreth, 1980; Birch et al., 2010) with biased-adaptation-related features. In detail, we retrofitted this static model by adding adaptation-strength-related decaying factors to both Gaussian components, making it dynamically transformable with the strength of adaptation.

In the classical DoG model, positive and negative Gaussian components represent the spatial response tuning curves of excitatory center and inhibitory surround of RF, respectively. When the spatial control factor (σ_1) of the positive component was smaller than that of the negative component (σ_2), the summation of two Gaussian-components could exhibit classical center-surround RF structure (Fig. 5A; example parameters, $a_1 = 1.0$, $a_2 = -2.0$, $\sigma_1 = 1$, $\sigma_2 = 5$; see above, Materials and Methods).

After that, both positive and negative Gaussian components were set to decay with the increasing biased-adaptation probabilities. According to previous reports (Cavanaugh et al., 2002; Patterson et al., 2013), decay functions were exponentially shaped, with different decay factors (b_1 for positive Gaussian component, b_2 for negative Gaussian component) and magnitude factors (c_1 for positive Gaussian component, c_2 for negative

Gaussian component) to simulate the adaptation sensitivity of RF center and surround subareas (Fig. 5B; see above, Materials and Methods). In the model, the decay speed of the negative Gaussian component is faster than that of the positive Gaussian component ($b_2 > b_1$); thus the suppression of RF surround is greater at low BAP. Meanwhile, the decay magnitude of the positive Gaussian component is greater than that of the negative Gaussian component ($c_1 > c_2$); thus the RF center component plays a dominant role at high BAP. At low BAP, the negative Gaussian component is suppressed more than the positive Gaussian component, leading to potentiation of the overall response, whereas at high BAP, the positive Gaussian component is suppressed more than the negative Gaussian component, leading to suppression of the overall response. Therefore, this model could simulate the bidirectional modulation of neural response during biased adaptation.

To verify the goodness of this model, we fitted the experimental data (peak response change ratios of Area 17 neurons) and obtained satisfying results. The bidirectional-plasticity feature of two individual Area 17 neurons could be well reproduced by this model (Fig. 5C). We fitted all the bidirectional-plastic neurons with sufficient data points (≥ 4), and a population distribution of R^2 (0.86 ± 0.02 , $n = 59$) suggests overall goodness of fit (Fig. 5D). Moreover, experimental results showed a minority (27%) of Area 17 neurons exhibited the adaptation-only feature after biased adaptation, and we found this model could also reproduce the peak response change ratios of the adaptation-only neuron (Fig. 5E) with acceptable goodness (Fig. 5F; $R^2 = 0.89 \pm 0.03$, $n = 19$) by setting the magnitude factor of the negative Gaussian component (c_2) to minimum, which is equivalent to removing the RF surround modulation effect. These findings suggest the effectiveness of the model in simulating the experimental bidirectional-plasticity feature as well as its compatibility with classical suppressive-only adaptation effects.

To further investigate effectiveness of this model in reproducing experimental population results and to determine corresponding optimal simulation parameters, we fitted the experimental population peak response change ratios of Area 17 neurons (Fig. 1H) with this model and obtained satisfying results (Fig. 5G). The corresponding optimal simulation parameters are (1) gain control factors of RF Gaussian components, $a_1 = 1.0$, $a_2 = -2.0$; (2) spatial control factors of RF Gaussian-components, $\sigma_1 = 1$, $\sigma_2 = 5$; (3) decay factors of decay functions, $b_1 = 6.56$, $b_2 = 16.19$; and (4) magnitude factors of decay functions, $c_1 = 22.56$, $c_2 = 20.13$ (see above, Materials and Methods).

To explore the relationship between parameter settings and the bidirectional-plastic modulation effect, we analyzed the parameter spaces focusing on the impact of magnitude factors (c) and decay factors (b) on neural peak response change ratios (%), especially at low (BAP = 0.18) and high (BAP = 0.79) adaptation intensities. Proper parameter settings should reproduce the experimental result that bidirectional-plastic neurons were moderately potentiated at BAP 0.18 and moderately suppressed at BAP 0.79. Therefore, we examined the parameter spaces to ascertain if the parameters were meeting the above requirements by finding the intersection of parameters that could both induce moderate potentiation (0 ~ 40%) and moderate suppression (-40 ~ 0%) at BAP 0.18 and 0.79, respectively.

By fixing the decay factors at the optimal condition for population simulation ($b_1 = 6.56$, $b_2 = 16.19$), we calculated the neural peak response change ratios under different magnitude factors (c_1 and c_2 , range = 15 ~ 25, step = 0.2) and found proper

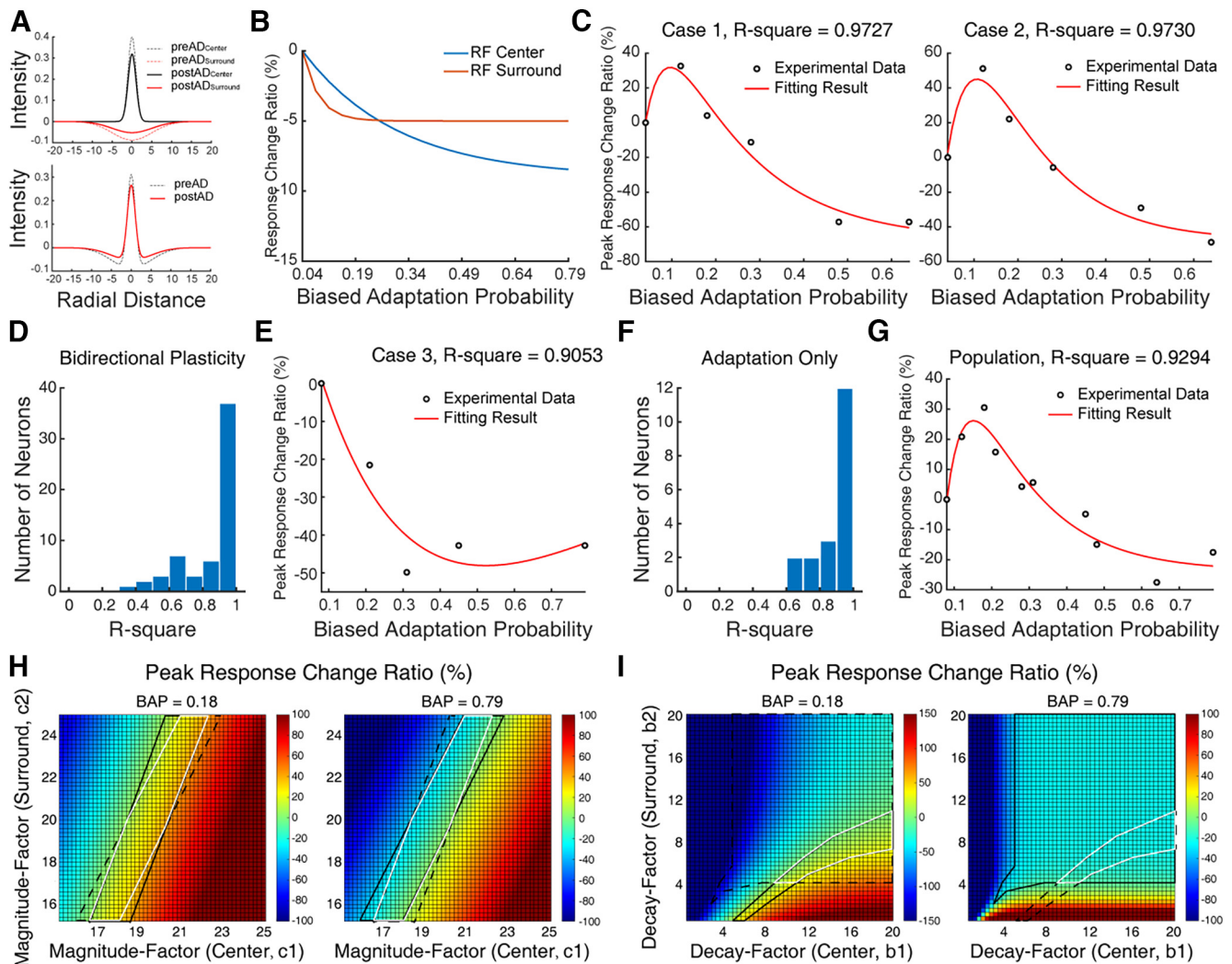


Figure 5. Simulation of the receptive field adaptation competition model. **A**, Schematic diagram of RF center-surround components (top) and overall RF structures (bottom) before (dotted line) and after (solid line) adaptation. **B**, Schematic diagram of decay functions of RF center and surround components during biased adaptation. Blue line indicates the response change ratio of RF center, and red line indicates that of RF surround. **C**, Two typical fitting results of bidirectional plastic Area 17 neurons using the RF adaptation-competition model. Black circles indicate experimental data, whereas red curves indicate fitting result. **D**, Histogram of fitting quality (R^2) for bidirectional plastic Area 17 neurons. **E**, Same as **C** of an adaptation-only Area 17 neuron. **F**, Same as **D** of adaptation-only Area 17 neurons. **G**, Fitting results of population peak response change ratio curve of Area 17 neurons using the RF adaptation competition model. Black circles indicate experimental data, whereas red curve indicates fitting result. **H**, The parameter spaces showing the neural peak response change ratios under different magnitude factors (decay factors fixed). Left, Parameter space at BAP 0.18. Right, Parameter space at BAP 0.79. Black solid frames indicate proper parameter ranges of each subgraph, whereas black dashed frames indicate proper parameter ranges of the other subgraph, so that there is a 0% ~ 40% increase at BAP 0.18 and a -40% ~ 0% change at BAP 0.79. White frames in two subgraphs indicate the intersection of proper parameter ranges. **I**, Same as **H** of decay factors (magnitude factors fixed).

magnitude factors for inducing moderate potentiation (Fig. 5H, left, black solid frame) and moderate suppression (Fig. 5H, right, black solid frame). The intersection of proper magnitude factors (Fig. 5H, white frames) is suitable for modeling the experimental results.

By fixing the magnitude factors at the optimal condition for population simulation ($c_1 = 22.56$, $c_2 = 20.13$), we calculated the neural peak response change ratios under different decay factors (b_1 and b_2 , range = 0 ~ 20, step = 0.4) and found proper decay factors for inducing moderate potentiation (Fig. 5I, left, black solid frame) and moderate suppression (Fig. 5I, right, black solid frame). The intersection of proper decay factors (Fig. 5I, white frames) is suitable for modeling the experimental results.

Together, the above simulation results provide evidence supporting the goodness of our RF center-surround adaptation-competition hypothesis.

Saliency detection

Saliency detection is essential for information processing. During this process, the novelty of a specific element within a complex background could be quantified by occurrence probability; higher probability indicates higher ordinary (redundancy, which needs to be suppressed), whereas lower probability indicates higher novelty (which needs to be potentiated). Within a time window, the occurrence-probability-dependent bidirectional modulation of neural responsiveness we found in this work would lead to response potentiation of novel stimulus and response suppression of redundant stimulus. As a result, it will help the temporal novelty detection. We thus hypothesize that the short-term bidirectional-plasticity in visual thalamo-ventral pathway may provide the neural mechanism of saliency detection (Li, 2002, 2019) of temporal-statistically distributed visual stream inputs.

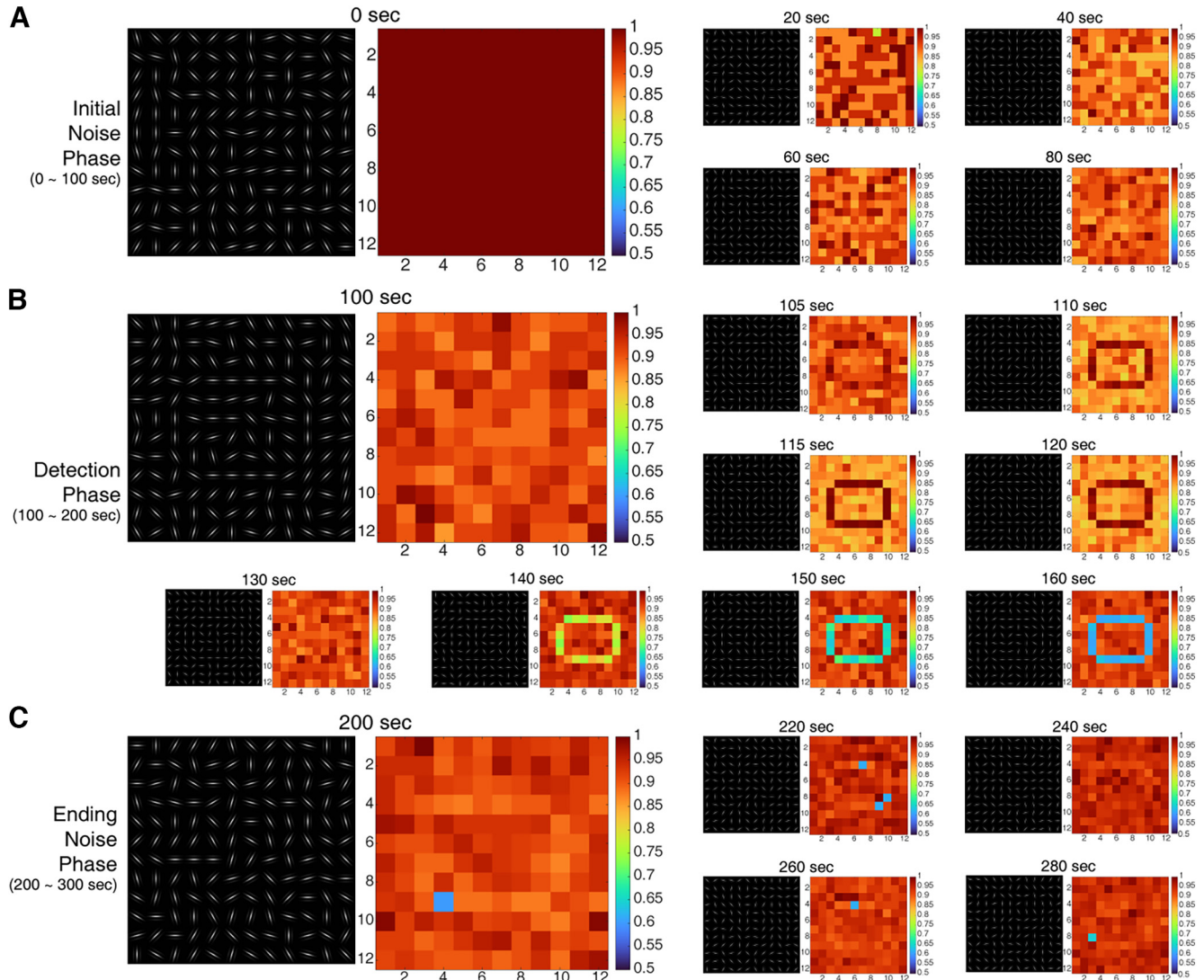


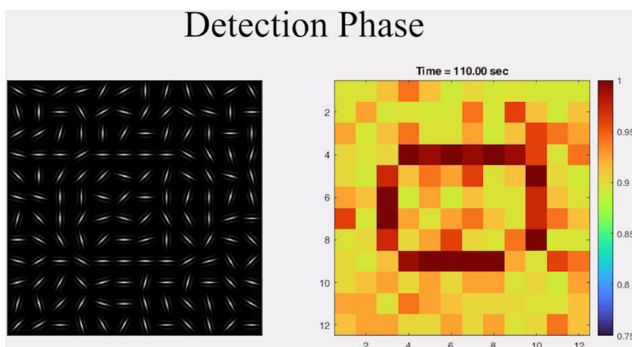
Figure 6. Saliency maps (Area 17) during dynamic visual inputs. **A**, Initial noise phase (0 ~ 100 s). **B**, Detection phase (100 ~ 200 s). **C**, Ending noise phase (200 ~ 300 s). Each sample consists of two parts, the left part is visual input, and the right part is a corresponding saliency map. Duration of each stimulus is 0.5 s with a 0.5 s blank interval (300 stimuli last for 300 s, and each phase lasts 100 s). Full video can be found in Movie 1.

To verify this hypothesis, we performed simulation of saliency detection, based on occurrence-probability-dependent short-term bidirectional-plasticity properties of Area 17 neurons. According to saliency detection theory, the saliency value of each visual location was calculated as its corresponding neural response intensity relative to the highest response intensities of other surrounding locations (Li, 2019), and the saliency values of the entire visual field could form a saliency map. Therefore, by temporally modulating relative neural responses during a period of time (based on the occurrence-probability-dependent neural bidirectional-plasticity), saliency detection of dynamic visual inputs could be performed.

In simulation, neuron clusters (whose population RFs covered the entire visual field) were exposed to a visual stream frame by frame (each frame lasted for 0.5 s with 0.5 s blank intervals, identical to experimental protocol) composed of three successive phases (each lasting for 100 frames), initial noise, detection, and ending noise (Fig. 6). During the initial and ending noise phases, neuron clusters received randomized unbiased orientation stimuli of bars as a simulation of noisy context visual stream inputs. During the detection phase, a stable elliptical contour repetitively

(frame by frame) appeared in the visual field, thus modulating the responses of corresponding neuron clusters. Over time, the cumulative occurrence probabilities of stimulating bars gradually changed and induced modulation of neural responses because of V1 bidirectional-plasticity properties revealed by experiments (bidirectional-plasticity function obtained by the RF center-surround adaptation-competition model described above; see above, Materials and Methods). The sliding time window used for calculating occurrence probability and its related neural response modulation is 10 min, suggested by the experimental bidirectional-plasticity time course (Fig. 1K).

During the initial and ending noise phases, no particular change occurred in the saliency map (Fig. 6A,C). However, during the detection phase (Fig. 6B, Movie 1), the saliency values continuously changed at locations where the elliptical contour appeared (because the occurrence probabilities of corresponding locations kept refreshing and accumulating frame by frame, and thus the one of contour orientation increased with time). During 0 ~ 20 s (0 ~ 20 frames) after stimulus onset, the occurrence probability gradually increased from 0 to 0.18, and meanwhile the relative saliency values of stimulus also increased because of



Movie 1. Saliency map of dynamic visual input based on V1 bidirectional-plasticity feature. Left, Dynamic visual input consists of gratings. Right, Saliency map of dynamic visual input (left). Only stimulus-containing frames are shown in the movie, and each stimulus lasts for 0.5 s with a 0.5 s blank interval. Duration, initial noise phase = 100 s, detection phase = 100 s, ending noise phase = 100 s. The video is played at 10 \times speed (length = 30 s). Some frames in this movie are shown in Figure 6. [View online]

the potentiating modulation of the bidirectional-plasticity function (Fig. 6*B*; from 100 s to 120 s). During 20 ~ 30 s (20 ~ 30 frames) after stimulus onset, the occurrence probability continuously increased from 0.18 to 0.26, and meanwhile the relative saliency values of the stimulus decreased to the context level (Fig. 6*B*; 130 s). During 30 ~ 100 s (30 ~ 100 frames) after stimulus onset, the occurrence probability increased from 0.26 to 0.52, and meanwhile the relative saliency values of stimulus further decreased because of the suppressing modulation of bidirectional-plasticity function (Fig. 6*B*; after 140 s). Clearly, the time-dependent bidirectional modulation enhances the novelty information of stimulus and reduces the redundant information. By detecting the changes of the saliency map, novel targets could pop up from the context, which is helpful for further selection of visual inputs. We noticed that during the ending noise phase, saliency values of some locations (that displayed elliptical contour in the detection phase) exhibited suppression when identical orientations (displayed during the detection phase) randomly reoccurred. This suppression resulted from the aftereffect of the detection phase, which was maintained during the ending noise phase.

To further explore the difference in the saliency detection property between Area 17 and LGN, we repeated this simulation with the LGN version of bidirectional-plasticity function (obtained by the smoothing spline method with satisfying fitting quality of individual LGN neurons; Fig. 7*A*; see above, Materials and Methods). After applying this function in the saliency detection algorithm, we found that the distinct bidirectional-plastic properties of Area 17 and LGN lead to distinct time scales of saliency detection dynamics (Movie 2, notice the time label). With a similar stimulation design (however, for LGN, detection phase was prolonged to 800 frames), we found that the dynamics of LGN neuronal saliency detection is much slower than that of Area 17. LGN neurons need more time to finalize the potentiating modulation of visual inputs, 470 s (Fig. 7*C*, 570 s) for LGN and 30 s (Fig. 6*B*, 130 s) for Area 17 (time after stimulus onset), suggesting different strategies of information filtering and coding.

We also simulated the saliency detection of Area 21a neurons to further check the potential differences across LGN and Areas 17 and 21a. The population bidirectional-plasticity function of Area 21a was fitted by the smoothing spline method instead of the RF center-surround adaptation-competition model (Fig. 7*B*), for it was currently unclear whether the bidirectional-plasticity

of Area 21a neurons was RF structure-dependent. We found during the detection phase (Movie 3, Fig. 7*D*), Area 21a neurons only took ~15 s to finalize the potentiating modulation of visual inputs (470 s for LGN, 30 s for Area 17).

Together, the short-term bidirectional-plasticity in visual thalamo-ventral pathway may contribute to the saliency detection of temporal statistically distributed visual stream inputs.

Discussion

In this study we found single neuronal short-term bidirectional-plasticity induced by biased adaptation in visual thalamo-ventral pathway (LGN, Area 17, Area 21a) with a hierarchical decrease of maximal potentiation-inducing biased-adaptation probability (Fig. 4*L*). When various stimuli were randomly presented, the one with slightly higher occurrence probability would unexpectedly induce a potentiated instead of suppressed response, demonstrating a remarkable temporal dynamics of neuronal response. In Area 17 this potentiation was pattern-feature selective but interocularly transferable, RF-structure dependent, and primarily occurs 100–200 ms after stimulation onset. Furthermore, the potentiation in LGN could be eliminated by Area 17 lesion. These findings suggested the potentiation part of bidirectional-plasticity is possibly mainly originated from V1. Combined with simulation, we proposed the RF center-surround adaptation-competition model and argued this bidirectional-plasticity contributes to the saliency detection of temporal statistically distributed visual inputs.

Bidirectional-plasticity induced by biased orientation

adaptation, different effects compared with previous studies

In our study, the direction of neuronal modulation induced by biased orientation adaptation is highly related to BAP. We noticed that previous V1 studies (Benucci et al., 2013; Snow et al., 2016; Westrick et al., 2016) using biased orientation adaptation did not find potentiation effect. In fact, in the above studies, BAP was > 0.3 , which also could not induce potentiation in our study (Fig. 1*H*). Furthermore, our findings in Area 17 showed the proper range of potentiation-inducing BAP was 0.12 ~ 0.21. As for classical top-up or continuous adaptation protocol, the occurrence probability of an adaptor is 0.89 ~ 1, which would induce a robust adaptive suppression effect according to our results. Thus, our findings are consistent with previous studies under relatively high occurrence probability but extend the sphere of adaptation protocol and illustrate novel potentiation effect when the occurrence probability of adaptor is not too high.

RF center-surround interaction underlies the pattern-feature selectivity and formation of potentiation

In this study, we found pattern-feature selectivity of potentiation and proposed the RF center-surround adaptation-competition hypothesis. Pattern-feature selectivity of potentiation was consistent with the BAP dependence of RF surround modulation. We also found nonoptimal (weak) stimulus (covering RF classical center and extended surround) could not induce potentiation (which requires adaptation of suppressive RF surround according to our model). In fact, under strong RF center (classical center, the same below) activation, RF surround (extended surround, the same below) would be suppressive, whereas under weak RF-center activation, RF surround would be facilitating under weak stimulation (Ichida et al., 2007; Shushruth et al., 2012; Angelucci et al., 2017). Therefore,

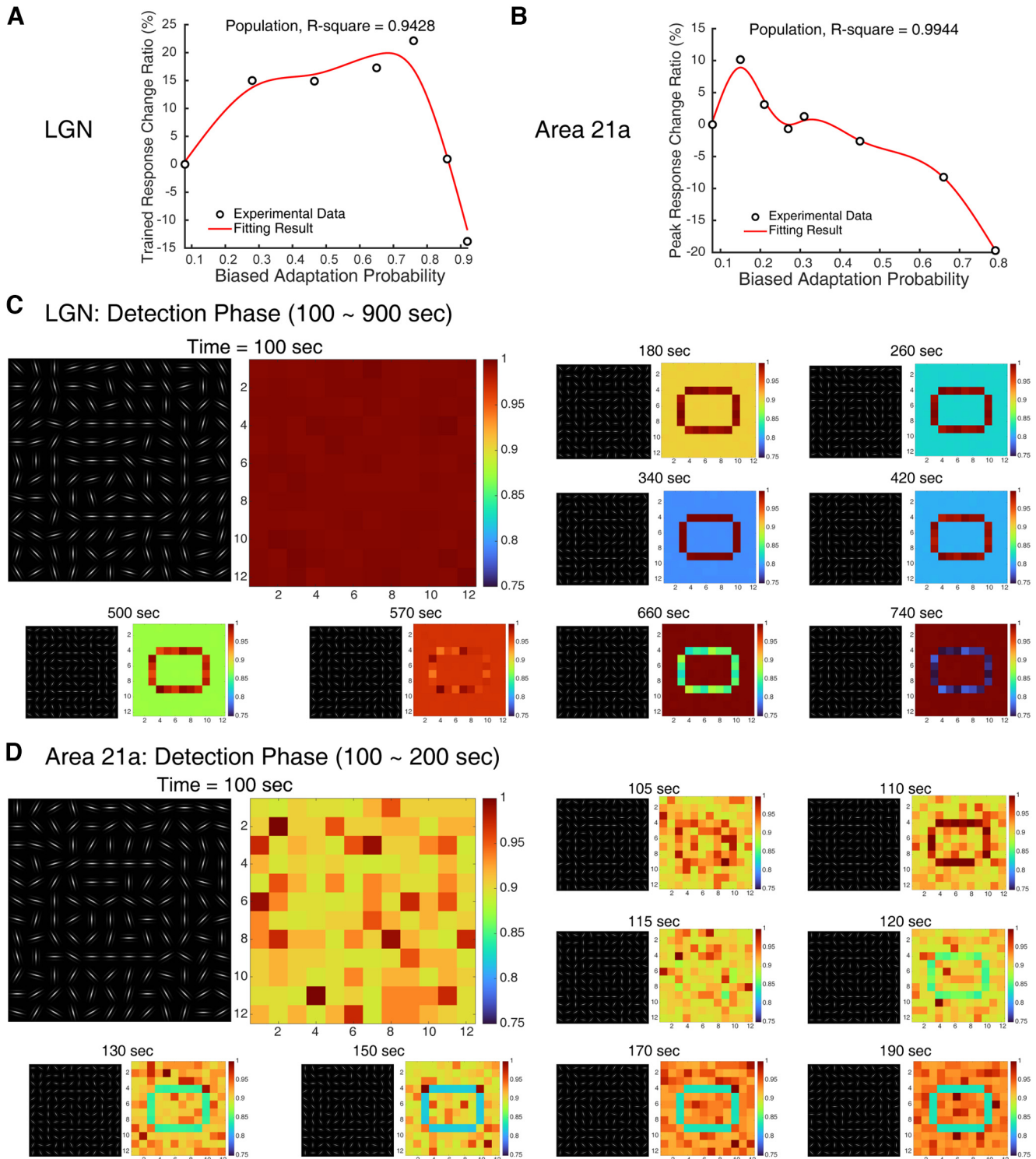
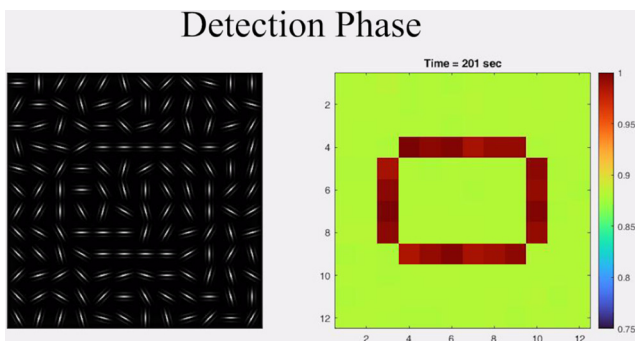


Figure 7. Saliency detection model of LGN and Area 21a. **A**, Fitting result of population trained response change ratio curve of LGN neurons, using the smoothing spline method. Black circles indicate experimental data, and red curve indicates fitting result. **B**, Same as **A** of Area 21a neurons. **C**, Saliency maps of LGN during the detection phase of dynamic visual inputs; each sample consists of two parts, the left part is visual input, and the right part is the corresponding saliency map. Duration of each stimulus is 0.5 s with a 0.5 s blank interval. **D**, Same as **C** of Area 21a. Full video can be found in Movies 2 and 3. It is notable that in **C** and **D**, the detection phase followed a 100 s initial phase, so the detection phase started from 100 s.

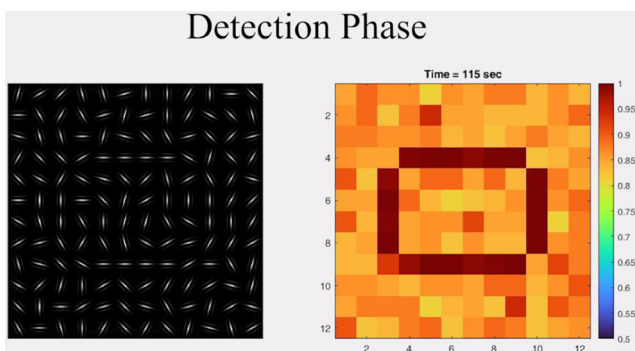
under a weak-stimulation condition, Area 17 neurons could not exhibit potentiation because of the lack of suppressive RF surround.

The adaptation sensitivity of RF surround is different with RF center. In our model, the relative adaptation sensitivities of RF center and surround during biased adaptation are important for

the formation of bidirectional-plasticity. In fact, Cavanaugh et al. (2002) combined the ratio of Gaussian model with contrast adaptation and found distinct sensitivities between RF center and surround. Later studies on contrast adaptation suggested identical results by pure or model-combined experiments (Dhruv et al., 2011; Wissig and Kohn, 2012).



Movie 2. Saliency map of dynamic visual input based on LGN bidirectional-plasticity feature. Left, Dynamic visual input consists of gratings. Right, Saliency map of dynamic visual input (left). Only stimulus-containing frames are shown in the movie, and each stimulus lasts for 0.5 s with a 0.5 s blank interval. Duration, initial noise phase = 100 s, detection phase = 800 s, ending noise phase = 100 s. The video is played at 40× speed (length = 25 s). Some frames in this movie are shown in Figure 7C. [View online]



Movie 3. Saliency map of dynamic visual input based on Area 21a bidirectional-plasticity feature. Left, Dynamic visual input consists of gratings. Right, Saliency map of dynamic visual input (left). Only stimulus-containing frames are shown in the movie, and each stimulus lasts for 0.5 s with a 0.5 s blank-interval. Duration, initial noise phase = 100 s, detection phase = 100 s, ending noise phase = 100 s. The video is played at 10× speed (length = 30 s). Some frames in this movie are shown in Figure 7D. [View online]

The hierarchical progressive propagation of bidirectional-plasticity from Area 17 to LGN and Area 21a

In this study we found that the potentiation induced by biased adaptation is originated in Area 17, supported by the interocular-transfer experiment, latency-analysis, and Area 17 lesion. Interocular transferability is useful when locating a visual function, especially in cats (Peck et al., 1979; Maffei et al., 1986), because LGN neurons are monocular driven, whereas Area 17 neurons of cats are mainly binocular driven (Hubel and Wiesel, 1962; Kasamatsu and Imamura, 2020). Latency analysis is a classical method for investigating the origin of sensory neuronal response (Angelucci and Bullier, 2003; Patterson et al., 2013; Yao et al., 2015), and our results suggest the intracortical origin of potentiation. The elimination of potentiation effect in LGN after Area 17 lesion further supports the Area 17 origin hypothesis.

In this study we found bidirectional-plasticity in LGN and confirmed its cortical origin by latency analysis and Area 17 lesion. LGN receives massive excitatory feedback from Area 17 (Andolina et al., 2013; Ichida et al., 2014; Wang et al., 2018), which has direct excitatory (through LGN relay neurons) and indirect inhibitory (through LGN inhibitory interneurons and Thalamic Reticular Nucleus (TRN) inhibitory projection) effects on LGN neurons (Ichida and Casagrande, 2002; Jurgens et al., 2012). Meanwhile, we also found that LGN neurons exhibited

strong potentiation at BAP $0.48 \sim 0.78$ (during which cortical neurons were suppressed), indicating complex cortical feedback mechanisms. It is possible that (1) during low BAP, cortical neuronal responses were potentiated, and cortical-feedback might be excitatory, leading to stronger excitation of LGN, and (2) during higher BAP ($0.48 \sim 0.78$), cortical feedback to TRN (Guillery et al., 1998; Pinault, 2004) might be suppressed, leading to disinhibition of TRN to LGN, also resulting in stronger excitation of LGN. Further in-depth investigation is required to verify this presumption.

In this study we found propagation of potentiation effect from Area 17 to Area 21a, with the following two possible mechanisms: (1) Area 21a neurons simply inherit bidirectional-plastic features from Area 17 and integrate it with intrinsic plasticity-properties, and (2) from Area 17 to Area 21a, the relative adaptation-sensitivity of RF surround might be weakened. The first mechanism is consistent with the linear-nonlinear-Poisson model (Paninski, 2004), which reproduced the enhancement of adaptation aftereffect along visual pathway. However, the impacts of horizontal/feedback connections were absent. The second mechanism involves local network mechanisms, especially the weakening of surround modulation, which might result from the sparse and fragmented horizontal connections of higher cortex (Cohen and Kohn, 2011; Smith and Sommer, 2013; Goris et al., 2014; Solomon et al., 2015; Fernandez-Leon et al., 2018). We suggest that both mechanisms might be necessary for understanding bidirectional-plasticity propagation from Area 17 to Area 21a, and further examination is required.

Using latency analysis, we also found a hierarchical trend from LGN to Area 21a during the middle- and late epoch (Figs. 3A–C, 4E,K); as the hierarchy increased, the potentiation effect gradually diminished, whereas the suppression effect was enhanced. This finding was consistent with previous reports that the suppressive adaptation effect could be facilitated along the visual pathway (Dhruv and Carandini, 2014; Li et al., 2017; Meng et al., 2018) and provided preliminary evidence related to intrinsic or feedback influences, suggesting a complicated systematic pattern.

Saliency detection of dynamic visual stream by bidirectional plasticity

In this study we combined experimental evidences with computing simulations and suggested that the bidirectional-plasticity is a promising mechanism of visual stream saliency detection. Previous studies on saliency detection mainly focused on spatial-distributed visual inputs, interpreting the pop out of a salient target as the result of RF surround modulation (Li, 1999; Coen-Cagli et al., 2012; Yan et al., 2018) or suppressive-only adaptation (McDermott et al., 2010; Dutta et al., 2016; Pojoga et al., 2020). In addition to that, saliency detection of the temporal-distributed visual stream is also in great need, especially in natural scenes. However, classical adaptation protocol is not very suitable for representing the temporal-statistically distributed visual inputs (Wissig et al., 2013). In this study, we adopted biased-adaptation protocol and found that the response potentiation/suppression of novel/redundant stimulus could contribute to the pop out of key elements within dynamic visual stream (Fig. 6B, Movie 1). Moreover, the pattern-feature selectivity of potentiation could further increase the signal-to-noise ratio of saliency detection.

In our study cortical feedback to LGN potentially enhances visual stream saliency detection by altering early information inputs, consistent with previous studies that cortical feedback

influences the spatial-temporal coding feature of LGN (Cudeiro and Sillito, 1996; Wang et al., 2006; Andolina et al., 2013; Wang et al., 2018), making LGN a spatial-temporal filter to enhance feature-specific inputs according to significance suggested by cortex (Wrobel, 2000; Carandini et al., 2007; Bayram et al., 2016; Han and VanRullen, 2016). Our finding further demonstrated the distinct bidirectional-plastic properties, which led to different visual-detection strategies of LGN and V1 (Fig. 7C, Movie 2). In LGN it is easier to potentiate response induced by a repetitively presented adaptor, making it easier to pop out in saliency map, whereas the suppression need much higher occurrence probability. This strategy helps the subcortical LGN encode richer information, based on which the downstream V1 could further select useful content. Consistent with this idea, adaptive suppression was further enhanced in Area 21a in our experiment, leading to sparser information coding. That means that even for the same visual stream, different brain regions provide different saliency maps. It is notable that the early epoch potentiation in some LGN neurons also suggested an alternative circuit hypothesis involving subcortical areas like the SC, which could encode visual saliency before V1 (White et al., 2017) and project to LGN (Liu et al., 2022), which might contribute to the saliency-coding feature of LGN and V1. However, there are also arguments that the saliency detection started in V1, regarding the SC as its downstream (Yan et al., 2018; Li, 2019; Zhaoping, 2022), and further investigation is still needed.

Together, the occurrence-probability-dependent neuronal bidirectional-plasticity of Area 21a neurons is a promising neural mechanism of the visual stream saliency detection, contributing to our understandings of bottom-up efficient coding of dynamic natural visual inputs by visual system.

References

- Andolina IM, Jones HE, Sillito AM (2013) Effects of cortical feedback on the spatial properties of relay cells in the lateral geniculate nucleus. *J Neurophysiol* 109:889–899.
- Angelucci A, Bullier J (2003) Reaching beyond the classical receptive field of V1 neurons: horizontal or feedback axons? *J Physiol Paris* 97:141–154.
- Angelucci A, Bijanzadeh M, Nurminen L, Federer F, Merlin S, Bressloff PC (2017) Circuits and mechanisms for surround modulation in visual cortex. *Annu Rev Neurosci* 40: 425–451.
- Bachatene L, Bharmauria V, Rouat J, Molotchnikoff S (2012) Adaptation-induced plasticity and spike waveforms in cat visual cortex. *NeuroReport* 23:88–92.
- Bair W, Cavanaugh JR, Cavanaugh JR, Movshon JA (2003) Time course and time-distance relationships for surround suppression in macaque V1 neurons. *J Neurosci* 23:7690–7701.
- Bayram A, Karahan E, Bilgiç B, Ademoglu A, Demiralp T (2016) Achromatic temporal-frequency responses of human lateral geniculate nucleus and primary visual cortex. *Vision Res* 127:177–185.
- Benjamini Y, Hochberg Y (1995) Controlling the false discovery rate: a practical and powerful approach to multiple testing. *J R Stat Soc B Methodological* 57:289–300.
- Benucci A, Saleem AB, Carandini M (2013) Adaptation maintains population homeostasis in primary visual cortex. *Nat Neurosci* 16:724–729.
- Birch P, Mitra B, Bangalore NM, Rehman S, Young R, Chatwin C (2010) Approximate bandpass and frequency response models of the difference of Gaussian filter. *Opt Commun* 283:4942–4948.
- Brainard DH (1997) The Psychophysics Toolbox. *Spat Vis* 10:433–436.
- Cang J, Kalatsky VA, Löwel S, Stryker MP (2005) Optical imaging of the intrinsic signal as a measure of cortical plasticity in the mouse. *Vis Neurosci* 22:685–691.
- Carandini M, Movshon JA, Ferster D (1998) Pattern adaptation and cross-orientation interactions in the primary visual cortex. *Neuropharmacology* 37:501–511.
- Carandini M, Horton JC, Sincich LC (2007) Thalamic filtering of retinal spike trains by postsynaptic summation. *J Vis* 7(14):20 1–11.
- Cattan S, Bachatene L, Bharmauria V, Jeyabalaratnam J, Milleret C, Molotchnikoff S (2014) Comparative analysis of orientation maps in areas 17 and 18 of the cat primary visual cortex following adaptation. *Eur J Neurosci* 40:2554–2563.
- Cavanaugh JR, Bair W, Movshon JA (2002) Nature and interaction of signals from the receptive field center and surround in macaque V1 neurons. *J Neurophysiol* 88:2530–2546.
- Clifford CW, Webster MA, Stanley GB, Stocker AA, Kohn A, Sharpee TO, Schwartz O (2007) Visual adaptation: neural, psychological and computational aspects. *Vision Res* 47:3125–3131.
- Cohen MR, Kohn A (2011) Measuring and interpreting neuronal correlations. *Nat Neurosci* 14:811–819.
- Coen-Cagli R, Dayan P, Schwartz O (2012) Cortical surround interactions and perceptual salience via natural scene statistics. *PLoS Comput Biol* 8: e1002405.
- Cudeiro J, Sillito AM (1996) Spatial frequency tuning of orientation-discontinuity-sensitive corticofugal feedback to the cat lateral geniculate nucleus. *J Physiol* 490:481–492.
- Daniels JD, Norman J, Pettigrew JD (1977) Biases for oriented moving bars in lateral geniculate nucleus neurons of normal and stripe-reared cats. *Exp Brain Res* 29:155–172.
- De Valois RL, Albrecht DG, Thorell LG (1982) Spatial frequency selectivity of cells in macaque visual cortex. *Vis Res* 22:545–559.
- Dhruv NT, Carandini M (2014) Cascaded effects of spatial adaptation in the early visual system. *Neuron* 81:529–535.
- Dhruv NT, Tailby C, Sokol SH, Lennie P (2011) Multiple adaptable mechanisms early in the primate visual pathway. *J Neurosci* 31:15016–15025.
- Dragoi V, Sur M (2000) Dynamic properties of recurrent inhibition in primary visual cortex: contrast and orientation dependence of contextual effects. *J Neurophysiol* 83:1019–1030.
- Dragoi V, Sharma J, Miller EK, Sur M (2002) Dynamics of neuronal sensitivity in visual cortex and local feature discrimination. *Nat Neurosci* 5:883–891.
- Dreher B, Michalski A, Ho RH, Lee CW, Burke W (1993) Processing of form and motion in area 21a of cat visual cortex. *Vis Neurosci* 10:93–115.
- Durand S, Freeman TCB, Carandini M (2007) Temporal properties of surround suppression in cat primary visual cortex. *Vis Neurosci* 24:679–690.
- Dutta A, Wagner H, Gutfreund Y (2016) Responses to pop-out stimuli in the barn owl's optic tectum can emerge through stimulus-specific adaptation. *J Neurosci* 36:4876–4887.
- Erişir A, Van Horn SC, Sherman SM (1998) Distribution of synapses in the lateral geniculate nucleus of the cat: differences between laminae A and A1 and between relay cells and interneurons. *J Comp Neurol* 390:247–255.
- Felsen G, Shen Y, Yao H, Spor G, Li C, Dan Y (2002) Dynamic modification of cortical orientation tuning mediated by recurrent connections. *Neuron* 36:945–954.
- Fernandez-Leon JA, Hansen BJ, Dragoi V (2018) Representation of rapid image sequences in V4 networks. *Cereb Cortex* 28:2675–2684.
- Ghodrati M, Khaligh-Razavi S, Lehky SR (2017) Towards building a more complex view of the lateral geniculate nucleus: recent advances in understanding its role. *Prog Neurobiol* 156:214–255.
- Goris RLT, Movshon JA, Simoncelli EP (2014) Partitioning neuronal variability. *Nat Neurosci* 17:858–865.
- Guido W, Sherman SM (1998) Response latencies of cells in the cat's lateral geniculate nucleus are less variable during burst than tonic firing. *Vis Neurosci* 15: 231–237.
- Guillery RW (1969) The organization of synaptic interconnections in the laminae of the dorsal lateral geniculate nucleus of the cat. *Z Zellforsch Mikrosk Anat* 96: 1–38.
- Guillery RW, Feig SL, Lozsádi DA (1998) Paying attention to the thalamic reticular nucleus. *Trends Neurosci* 21:28–32.
- Han B, VanRullen R (2016) Shape perception enhances perceived contrast: evidence for excitatory predictive feedback? *Sci Rep* 6:22944.
- Henry CA, Joshi S, Xing D, Shapley RM, Hawken MJ (2013) Functional characterization of the extraclassical receptive field in macaque V1: contrast, orientation, and temporal dynamics. *J Neurosci* 33:6230–6242.
- Hu B, Li X, Shou T (2000) Effects of bicuculline on direction-sensitive relay cells in the dorsal lateral geniculate nucleus (LGnd) of cats. *Brain Res* 885:87–93.
- Hua T, Li X, He L, Zhou Y, Wang Y, Leventhal AG (2006) Functional degradation of visual cortical cells in old cats. *Neurobiol Aging* 27:155–162.

- Huang L, Chen X, Shou T (2004) Spatial frequency-dependent feedback of visual cortical area 21a modulating functional orientation column maps in areas 17 and 18 of the cat. *Brain Res* 998:194–201.
- Huang L, Shou T, Chen X, Yu H, Sun C, Liang Z (2006) Slab-like functional architecture of higher order cortical area 21a showing oblique effect of orientation preference in the cat. *Neuroimage* 32:1365–1374.
- Hubel DH, Wiesel TN (1962) Receptive fields, binocular interaction and functional architecture in the cat's visual cortex. *J Physiol* 160:106–154.
- Hyvärinen A, Hurri J, Väyrynen J (2004) A unifying framework for natural image statistics: spatiotemporal activity bubbles. *Neurocomputing* 58:60:801–806.
- Ichida JM, Casagrande VA (2002) Organization of the feedback pathway from striate cortex (V1) to the lateral geniculate nucleus (LGN) in the owl monkey (*Aotus trivirgatus*). *J Comp Neurol* 454:272–283.
- Ichida JM, Schwabe L, Bressloff PC, Angelucci A (2007) Response facilitation from the “suppressive” receptive field surround of macaque V1 neurons. *J Neurophysiol* 98:2168–2181.
- Ichida JM, Mavity-Hudson JA, Casagrande VA (2014) Distinct patterns of corticogeniculate feedback to different layers of the lateral geniculate nucleus. *Eye Brain* 2014:57–73.
- Jurgens CW, Bell KA, McQuiston AR, Guido W (2012) Optogenetic stimulation of the corticothalamic pathway affects relay cells and GABAergic neurons differently in the mouse visual thalamus. *PLoS One* 7:e45717.
- Kara P, Boyd JD (2009) A micro-architecture for binocular disparity and ocular dominance in visual cortex. *Nature* 458:627–631.
- Kasamatsu T, Imamura K (2020) Ocular dominance plasticity: molecular mechanisms revisited. *J Comp Neurol* 528:3039–3074.
- Kayser C, Einhäuser W, König P (2003) Temporal correlations of orientations in natural scenes. *Neurocomputing* 52–54:117–123.
- Kohn A (2007) Visual adaptation: physiology, mechanisms, and functional benefits. *J Neurophysiol* 97:3155–3164.
- Kohn A, Movshon JA (2004) Adaptation changes the direction tuning of macaque MT neurons. *Nat Neurosci* 7:764–772.
- Kuhlman SJ, Tring E, Trachtenberg JT (2011) Fast-spiking interneurons have an initial orientation bias that is lost with vision. *Nat Neurosci* 14:1121–1123.
- Lee J, Williford T, Maunsell JH (2007) Spatial attention and the latency of neuronal responses in macaque area V4. *J Neurosci* 27:9632–9637.
- LeVay S, Ferster D (1977) Relay cell classes in the lateral geniculate nucleus of the cat and the effects of visual deprivation. *J Comp Neurol* 172:563–584.
- Leventhal AG, Schmolesky MT, Pu M, Leventhal AG (2000) Degradation of stimulus selectivity of visual cortical cells in senescent rhesus monkeys. *Nat Neurosci* 3:384–390.
- Levick WR, Thibos LN (1982) Analysis of orientation bias in cat retina. *J Physiol* 329:243–261.
- Li CY, Li W (1994) Extensive integration field beyond the classical receptive field of cat's striate cortical neurons—classification and tuning properties. *Vis Res* 34:2337–2355.
- Li H, Fang Q, Ge Y, Li Z, Meng J, Zhu J, Yu H (2018) Relationship between the dynamics of orientation tuning and spatiotemporal receptive field structures of cat LGN neurons. *Neuroscience* 377:26–39.
- Li W, Thier P, Wehrhahn C (2001) Neuronal responses from beyond the classic receptive field in V1 of alert monkeys. *Exp Brain Res* 139:359–371.
- Li Z (1999) Contextual influences in V1 as a basis for pop out and asymmetry in visual search. *Proc Natl Acad Sci U S A* 96:10530–10535.
- Li Z (2002) A saliency map in primary visual cortex. *Trends Cogn Sci* 6:9–16.
- Li Z (2019) A new framework for understanding vision from the perspective of the primary visual cortex. *Curr Opin Neurobiol* 58:1–10.
- Li Z, Meng J, Li H, Jin A, Tang Q, Zhu J, Yu H (2017) The feature-specific propagation of orientation and direction adaptation from areas 17 to 21a in cats. *Sci Rep* 7:390–390.
- Liu X, Huang H, Snutch TP, Cao P, Wang L, Wang F (2022) The superior colliculus: cell types, connectivity, and behavior. *Neurosci Bull*
- Lu SM, Guido W, Vaughan JW, Sherman SM (1995) Latency variability of responses to visual stimuli in cells of the cat's lateral geniculate nucleus. *Exp Brain Res* 105:7–17.
- Lussiez R, Chanauria N, Ouelhazi A, Molotchnikoff S (2021) Effects of visual adaptation on orientation selectivity in cat secondary visual cortex. *Eur J Neurosci* 53:588–600.
- Maffei L, Fiorentini A, Bisti S (1973) Neural correlate of perceptual adaptation to gratings. *Science* 182:1036–1038.
- Maffei L, Berardi N, Bisti S (1986) Interocular transfer of adaptation after effect in neurons of area 17 and 18 of split chiasm cats. *J Neurophysiol* 55:966–976.
- Marr D, Hildreth E (1980) Theory of edge detection. *Proc R Soc Lond B Biol Sci* 207:187–217.
- McDermott KC, Malkoc G, Mulligan JB, Webster MA (2010) Adaptation and visual salience. *J Vis* 10(13):17.
- Meng J, Li Z, Li H, Zhu J, Yu H (2018) The common and distinct orientation adaptation effect at pinwheel centers in areas 21a and 17 of cats. *Neuroscience* 379:77–92.
- Montero VM (1991) A quantitative study of synaptic contacts on interneurons and relay cells of the cat lateral geniculate nucleus. *Exp Brain Res* 86:257–270.
- Morley JW, Vickery RM (1997) Spatial and temporal frequency selectivity of cells in area 21a of the cat. *J Physiol* 501:405–413.
- Movshon JA, Lennie P (1979) Pattern-selective adaptation in visual cortical neurones. *Nature* 278:850–852.
- Müller JR, Metha AB, Krauskopf J, Lennie P (1999) Rapid adaptation in visual cortex to the structure of images. *Science* 285: 1405–1408.
- Nowak LG, Munk MHJ, Girard P, Bullier J (1995) Visual latencies in areas V1 and V2 of the macaque monkey. *Vis Neurosci* 12: 371–384.
- Paninski L (2004) Maximum likelihood estimation of cascade point-process neural encoding models. *Network* 15:243–262.
- Patterson CA, Wissig SC, Kohn A (2013) Distinct effects of brief and prolonged adaptation on orientation tuning in primary visual cortex. *J Neurosci* 33:532–543.
- Patterson CA, Wissig SC, Kohn A (2014a) Adaptation disrupts motion integration in the primate dorsal stream. *Neuron* 81:674–686.
- Patterson CA, Duijnhouwer J, Wissig SC, Krekelberg B, Kohn A (2014b) Similar adaptation effects in primary visual cortex and area MT of the macaque monkey under matched stimulus conditions. *J Neurophysiol* 111:1203–1213.
- Peck CK, Crewther SG, Hamilton CR (1979) Partial interocular transfer of brightness and movement discrimination by split-brain cats. *Brain Res* 163:61–75.
- Pelli DG (1997) The VideoToolbox software for visual psychophysics: transforming numbers into movies. *Spatial Vis* 10:437–442.
- Pinault D (2004) The thalamic reticular nucleus: structure, function and concept. *Brain Res Brain Res Rev* 46:1–31.
- Pojoga SA, Kharas N, Dragoi V (2020) Perceptually unidentifiable stimuli influence cortical processing and behavioral performance. *Nat Commun* 11:6109.
- Raiquel SE, Lagae L, Orban GA (1989) Response latencies of visual cells in macaque areas V1, V2 and V5. *Brain Res* 493:155–159.
- Reinsch CH (1967) Smoothing by spline functions. *Numer Math* 10:177–183.
- Rieke F, Rudd ME (2009) The challenges natural images pose for visual adaptation. *Neuron* 64:605–616.
- Ruderman DL, Bialek W (1994) Statistics of natural images: scaling in the woods. *Phys Rev Lett* 73:814–817.
- Sanderson KJ (1971) The projection of the visual field to the lateral geniculate and medial interlaminar nuclei in the cat. *J Comp Neurol* 143:101–117.
- Saul AB, Cynader MS (1989) Adaptation in single units in visual cortex: the tuning of aftereffects in the spatial domain. *Vis Neurosci* 2:593–607.
- Schwartz O, Hsu A, Dayan P (2007) Space and time in visual context. *Nat Rev Neurosci* 8:522–535.
- Shapley RM, Xing D (2013) Local circuit inhibition in the cerebral cortex as the source of gain control and untuned suppression. *Neural Netw* 37:172–181.
- Shou TD, Leventhal AG (1989) Organized arrangement of orientation-sensitive relay cells in the cat's dorsal lateral geniculate nucleus. *J Neurosci* 9:4287–4302.
- Shou T, Li X, Zhou Y, Hu B (1996) Adaptation of visually evoked responses of relay cells in the dorsal lateral geniculate nucleus of the cat following prolonged exposure to drifting gratings. *Vis Neurosci* 13:605–613.
- Shushruth S, Mangapathy P, Ichida JM, Bressloff PC, Schwabe L, Angelucci A (2012) Strong recurrent networks compute the orientation tuning of surround modulation in the primate primary visual cortex. *J Neurosci* 32:308–321.
- Skottun BC, De Valois RL, Grosenick DH, Movshon JA, Albrecht DG, Bonds AB (1991) Classifying simple and complex cells on the basis of response modulation. *Vision Res* 31:1079–1086.

- Smith MA, Sommer MA (2013) Spatial and temporal scales of neuronal correlation in visual area V4. *J Neurosci* 33:5422–5432.
- Snow M, Coen-Cagli R, Schwartz O (2016) Specificity and timescales of cortical adaptation as inferences about natural movie statistics. *J Vis* 16(13):1.
- Solomon SG, Kohn A (2014) Moving sensory adaptation beyond suppressive effects in single neurons. *Curr Biol* 24:R1012–R1022.
- Solomon SS, Chen SC, Morley JW, Solomon SG (2015) Local and global correlations between neurons in the middle temporal area of primate visual cortex. *Cereb Cortex* 25:3182–3196.
- Sundberg KA, Mitchell JF, Gawne TJ, Reynolds JH (2012) Attention influences single unit and local field potential response latencies in visual cortical area V4. *J Neurosci* 32:16040–16050.
- Tolias AS, Keliris GA, Gawne TJ, Reynolds JH (2005) Neurons in macaque area V4 acquire directional tuning after adaptation to motion stimuli. *Nat Neurosci* 8:591–593.
- Tong L, Zhu B, Li Z, Shou T, Yu H (2011) Feedback from area 21a influences orientation but not direction maps in the primary visual cortex of the cat. *Neurosci Lett* 504: 141–145.
- Tong L, Xie Y, Li Z, Shou T, Yu H (2016) The temporal–spatial dynamics of feature maps during monocular deprivation revealed by chronic imaging and self-organization model simulation. *Neuroscience* 339:571–586.
- Torralba A, Oliva A (2003) Statistics of natural image categories. *Network* 14:391–412.
- Troy JB, Lennie P (1987) Detection latencies of X and Y type cells of the cat's dorsal lateral geniculate nucleus. *Exp Brain Res* 65:703–706.
- Van Der Gucht E, Vandesande F, Arcckens L (2001) Neurofilament protein: a selective marker for the architectonic parcellation of the visual cortex in adult cat brain. *J Comp Neurol* 441:345–368.
- Van Horn SC, Erisir A, Sherman SM (2000) Relative distribution of synapses in the A-laminae of the lateral geniculate nucleus of the cat. *J Comp Neurol* 416:509–520.
- Wang C, Waleszczyk WJ, Burke W, Dreher B (2000) Modulatory influence of feedback projections from area 21a on neuronal activities in striate cortex of the cat. *Cereb Cortex* 10:1217–1232.
- Wang J, Ni Z, Jin A, Yu T, Yu H (2019) Ocular dominance plasticity of areas 17 and 21a in the cat. *Front Neurosci* 13:1039.
- Wang T, Li Y, Andolina IM, Salt TE, Sillito AM (2020) Laminar subnetworks of response suppression in macaque primary visual cortex. *J Neurosci* 40:7436–7450.
- Wang W, Jones HE, Andolina IM, Salt TE, Sillito AM (2006) Functional alignment of feedback effects from visual cortex to thalamus. *Nat Neurosci* 9:1330–1336.
- Wang W, Andolina IM, Lu Y, Jones HE, Sillito AM (2018) Focal gain control of thalamic visual receptive fields by layer 6 corticothalamic feedback. *Cereb Cortex* 28: 267–280.
- Webster MA (2015) Visual adaptation. *Annual Review of Vision Science* 1:547–567.
- Westrick ZM, Heeger DJ, Landy MS (2016) Pattern adaptation and normalization reweighting. *J Neurosci* 36:9805–9816.
- Weyand TG (2016) The multifunctional lateral geniculate nucleus. *Rev Neurosci* 27:135–157.
- White BJ, Kan JY, Levy R, Itti L, Munoz DP (2017) Superior colliculus encodes visual saliency before the primary visual cortex. *Proc Natl Acad Sci U S A* 114:9451–9456.
- Wiesel TN, Hubel DH (1963) Single-cell responses in striate cortex of kittens deprived of vision in one eye. *J Neurophysiol* 26:1003–1017.
- Wissig SC, Kohn A (2012) The influence of surround suppression on adaptation effects in primary visual cortex. *J Neurophysiol* 107:3370–3384.
- Wissig SC, Patterson CA, Kohn A (2013) Adaptation improves performance on a visual search task. *J Vis* 13: 6.
- Wrobel A (2000) Beta activity: a carrier for visual attention. *Acta Neurobiol Exp (Wars)* 60:247–260.
- Xing D, Ringach DL, Hawken MJ, Shapley RM (2011) Untuned suppression makes a major contribution to the enhancement of orientation selectivity in macaque V1. *J Neurosci* 31:15972–15982.
- Yan Y, Zhaoping L, Li W (2018) Bottom-up saliency and top-down learning in the primary visual cortex of monkeys. *Proc Natl Acad Sci U S A* 115:10499–10504.
- Yao Z, Wang Z, Yuan N, Liang Z, Zhou Y (2015) Delayed signal transmission in area 17, area 18 and the posteromedial lateral suprasylvian area of aged cats. *Neuroscience* 289:358–366.
- Yu H, Majewska AK, Sur M (2011) Rapid experience-dependent plasticity of synapse function and structure in ferret visual cortex *in vivo*. *Proc Natl Acad Sci U S A* 108:21235–21240.
- Zhaoping L (2022) Parallel advantage: further evidence for bottom-up saliency computation by human primary visual cortex. *Perception* 51:60–69.
- Zhou Y, Leventhal AG, Thompson KG (1995) Visual deprivation does not affect the orientation and direction sensitivity of relay cells in the lateral geniculate nucleus of the cat. *J Neurosci* 15:689–698.